Convective distribution of dust over the Arabian Peninsula: the impact of model resolution

Jennie Bukowski[1], Susan C. van den Heever[1]

[1] Department of Atmospheric Science, Colorado State University, Fort Collins, CO

Correspondence to: Jennie Bukowski (jennie.bukowski@colostate.edu)

Abstract

Along the coasts of the Arabian Peninsula, convective dust storms are a considerable source of mineral dust to the atmosphere. Reliable predictions of convective dust events are necessary to determine their effects on air quality, visibility, and the radiation budget. In this study, the Weather Research and Forecasting Model coupled with Chemistry (WRF-Chem) is used to simulate a 2016 summertime dust event over the Arabian Peninsula and examine the variability in dust fields and associated vertical transport due to the choice of convective parameterization and convection-allowing versus parameterized convection. Simulations are run at 45 km and 15 km grid spacing with multiple cumulus parameterizations, and are compared to a 3 km simulation that permits explicit dry and moist convective processes. Five separate cumulus parameterizations at 15 km grid spacing were tested to quantify the spread across different parameterizations. Finally, the impact these variations have on radiation, specifically aerosol heating rates is also investigated.

On average, in these simulations the convection-permitting case produces higher quantities of dust than the parameterized cases in terms of dust uplift potential, vertical dust concentrations, and vertical dust fluxes. Major drivers of this discrepancy between the simulations stem from the convection-allowing case exhibiting higher surface windspeeds during convective activity, lower dust emission wind threshold velocities due to drier soil, and more frequent, stronger vertical velocities which transport dust aloft and increase the atmospheric lifetime of these particles. For aerosol heating rates in the lowest levels, the shortwave effect prevails in the convection-permitting case with a net cooling effect, whereas a longwave net warming effect is present in the parameterized cases. The spread in dust concentrations across cumulus parameterizations at the same grid resolution (15 km) is an order of magnitude lower than the impact of moving from parameterized towards explicit convection. We conclude that tuning dust emissions in coarse resolution simulations can only improve the results to first-order and cannot fully rectify the discrepancies originating from disparities in the representation of convective dust transport.

1) Introduction

Airborne mineral dust is an important atmospheric aerosol (Zender et al., 2004; Ginoux et al., 2012): dust reduces visibility (e.g. Mahowald et al., 2007; Baddock et al., 2014; Camino et al., 2015) and is detrimental to the human respiratory system (Prospero, 1999; van Donkelaar et al., 2010; Stafoggia et al., 2016), but also plays a vital role in

fertilizing iron-deficient maritime ecosystems (Martin, 1991; Bishop et al., 2002; Mahowald et al., 2005; Jickells and Moore, 2015). Dust particles function as cloud condensation nuclei (e.g. Lee et al., 2009; Manktelow et al., 2009; Twohy et al., 2009; Karydis et al., 2011) and ice nuclei (e.g. DeMott et al., 2003; Field et al., 2006; Knopf and Koop, 2006; Boose et al., 2016), thereby altering cloud development and properties. Furthermore, mineral dust is of interest due to its distinctive optical properties; dust both scatters and absorbs shortwave and longwave radiation (e.g. Tegen et al., 1996; Kinne et al., 2003; Dubovik et al., 2006) modifying atmospheric thermodynamics and the earth's energy budget in the process (e.g. Slingo et al., 2006; Sokolik and Toon, 2006; Heald et al., 2014).

The influence of atmospheric mineral dust is widespread in the weather and climate system, yet generating skillful forecasts of dust concentrations and their temporal and spatial evolution has been difficult to achieve. Several studies suggest that including the radiative effects of mineral dust in numerical weather prediction (NWP) could refine the radiation balance of these models and improve forecasts (Kischa et al., 2003; Haywood et al., 2005; Pérez et al., 2006). Advances in climate models have been made by incorporating time-varying dust sources and climate-dust feedbacks in the radiative forcing calculations (Kok et al., 2014; Woodage and Woodward, 2014; Kok et al., 2018). However, these potential improvements are contingent upon the quality of the dust model and initialization data, which models are known to be especially sensitive to. As such, substantial discrepancies exist across global models of similar resolution (Huneeus et al., 2011), and across regional models (Uno et al., 2006; Todd et al., 2008) in the magnitude of predicted dust flux from the surface to the atmosphere.

A major challenge in modeling dust processes is the scales of motion involved in its emission and subsequent transport. Dust particles mobilize from the surface due to wind erosion of arid soils, a mechanism that occurs on the micron scale, but once airborne mineral dust can deposit locally or be transported on the synoptic to global scales. Dust events initiate from both large-scale and synoptic dynamical flow regimes, as well as mesoscale features. Synoptic scale uplift phenomena include monsoon troughs (e.g. Marsham et al., 2008), Shamal winds (e.g. Yu et al., 2015) and frontal systems (e.g. Beegum et al. 2018), while dynamical effects on smaller (meso) scales can raise dust through the production of convective outflow boundaries, or haboobs, (e.g. Miller et al. 2008), daytime turbulence or dry convective processes (e.g. Klose and Shao, 2012), and the morning mixing of nocturnal low level jet (NLLJ) momentum to the surface (e.g. Fiedler et al. 2013). When considering only meteorological dust sources, wind drives dust emissions, meaning that the underlying processes that contribute to the wind fields must be resolved in a model to create an accurate dust forecast.

One potential source of disagreement in models stems from the scaling emissions in dust parameterizations, which relate the surface emissions proportionally to the second or third power of surface windspeed. This means that minor miscalculations in modeled windspeeds go on to produce more substantial errors in the dust concentration calculations (e.g. Menut, 2008). Current aerosol forecast and climate models are run at fine enough grid-spacing to simulate synoptic events but still typically employ cumulus parameterizations, which are incapable of resolving dry and moist mesoscale updrafts and downdrafts that can potentially loft and / or scavenge dust. Schepanski et al. (2015) found that online dust models are likely to be most sensitive to the initialization data compared to other

67 model options, which adds additional uncertainty to dust forecasts. Pope et al. (2016) and Largeron et al. (2015)

68 both postulated that an inadequate representation of convection in coarse model simulations, specifically the

69 underestimation of high surface windspeeds in mesoscale haboobs, is a major contributor to errors in dust models.

70

71 The misrepresentation of dust concentrations in models with cumulus parameterizations has been investigated across

72 several modeling platforms, mostly from the perspective of dust lofting mechanisms at the surface. Heinold et al.

73 (2013) ran the UK Met Office Unified Model (UM) over West Africa with offline dust emissions, and found that of

74 the factors they tested, the model was most sensitive to explicit versus parameterized convection. Furthermore, in

75 the Heinhold et al. (2013) study, dust emissions were reduced as grid resolution was increased to convection-

76 permitting scales by roughly 50%. This was found to be due to the parameterized simulations underestimating moist

77 convective activity but drastically overestimating the NLLJ dust uplift mechanism, a similar relationship to that

78 originally identified in Marsham et al. (2011).

79 Conversely, studies using different numerical dust models have identified other relationships between horizontal

80 resolution and dust emissions. Roberts et al. 2018 also used UM to investigate this relationship over the Sahara and

81 Sahel and reported little change in the dust emissions when moving from parameterized to explicit convection, but

82 also noted that the NLLJ maximum decreased as the convective maximum increased. Reinfried et al. (2009)

83 simulated a haboob case study from Morocco with the Lokal Modell - MultiScale chemistry aerosol transport (LM-

84 MUSCAT, since renamed COSMO-MUSCAT) regional model and found increased dust emissions in a convection-

85 allowing simulation versus those with cumulus parameterizations. They also established that the model was more

86 sensitive to the choice of cumulus parameterization rather than the change in horizontal resolution. Similarly, Bouet

87 et al. (2012) identified an increase in dust emissions with increasing model resolution using the Regional

88 Atmospheric Modeling System coupled to the Dust Prediction Model (RAMS-DPM) while simulating a Bodélé

89 depression case study. Ridley et al. (2013) showed that global aerosol models with parameterized convection were

90 also sensitive to model resolution and that higher horizontal resolution led to higher dust emissions.

91

92 With the added computational expense of running aerosol code, the resolution of dust forecast models lags relative

93 to their weather-only prediction counterparts for both global and regional prediction systems (Benedetti et al., 2014;

94 Benedetti et al., 2018). Global dust forecasts generated by several aerosol models are available through the Sand and

95 Dust Storm Warning Advisory and Assessment System (SDS-WAS) (http://www.wmo.int/sdswas), but none

96 of the models in the SDS-WAS are currently run at fine enough grid-spacing to be considered convection-permitting

97 (SDS-WAS Model inter-comparison and forecast evaluation technical manual; last updated January, 2018). While

98 regional numerical weather prediction models have moved into convection-permitting scales, the added

99 computational cost of aerosol parameterizations means that convective parameterizations will be a necessity for

100 longer in models that employ online aerosol predictions. It is also clear that horizontal model resolution remains an

101 understudied factor in regional dust modeling. As such, exploring differences across cumulus parameterizations and

102 those relative to convection-permitting resolutions continues to be relevant and vital to better understand aerosol

103 forecasting and aerosol-cloud-environment interactions.

104   While previous studies have begun to examine the effect of horizontal model resolution on dust emissions and
105   airborne dust concentrations, there are several factors that warrant more investigation. As it stands, there is little
106   agreement on the sign of the response in dust emissions to a change in horizontal model resolution, which seems to
107   vary based on the regional model being utilized. Most studies have concentrated on the change in dust emissions
108   based on moving from parameterized convection to convection-allowing scales, while ignoring the possible
109   sensitivity due to the choice of the cumulus parameterization itself. Furthermore, much of the previous literature
110   focused on how the increase in resolution affects convective outflow boundaries and surface / near-surface processes
111   as dust sources, rather than convective transport and the vertical redistribution of dust and its radiative effects at
112   different levels of the atmosphere. In this paper, we seek to address these limitations in the understanding of the
113   effects of horizontal model resolution on dust concentrations. The goal of the research presented here is therefore to
114   quantify the sign and magnitude in the response of modeled dust fields in a regional numerical model to increasing
115   horizontal resolution.

116   In order to achieve our stated goal, we will use numerical simulations of a case study to examine the variability in
117   dust emissions and vertical dust concentrations and fluxes due to (1) the choice of convective parameterization, (2)
118   convection-allowing versus parameterized convection, and (3) the impact of these variations on radiation,
119   specifically aerosol heating rates. These simulations are performed using the Weather Research and Forecasting
120   Model coupled with Atmospheric Chemistry (WRF-Chem) (Skamarock et al., 2008; Grell et al., 2005; Fast et al.,
121   2006) a platform that has been tested for its sensitivity to vertical resolution for dust extinction coefficient profiles
122   (Teixeira et al., 2015) and horizontal model resolution and convective transport for chemical species such as carbon
123   monoxide (e.g. Klich and Fuelberg, 2013), but not for dust. These simulations will represent a case study of a
124   summertime coastal convective dust event over the Arabian Peninsula, a relatively understudied region compared to
125   areas such as the Sahara (Jish Prakash et al., 2015), despite being the world's second largest dust emission region
126   (Tanaka and Chiba, 2004).

127   This paper is part of a larger body of collaborative work conducted by the Holistic Analysis of Aerosols in Littoral
128   Environments (HAALE) research team under the Office of Naval Research Multidisciplinary Research Program of
129   the University Research Initiative (MURI). The primary goal of the HAALE-MURI project is to isolate the
130   fundamental environmental factors that govern the spatial distribution and optical properties of littoral zone aerosols.
131   The study discussed in this manuscript focuses on advancing our understanding in the role that convection plays in
132   the redistribution of dust aerosol and its radiative effects along the coast of arid regions, and seeks to quantify the
133   uncertainty in forecasted dust distributions stemming from the representation of convective processes in a regional
134   model.

135   The manuscript is organized as follows: an overview of the WRF-Chem model and physics setup (Sect. 2.1), dust
136   model setup (Sect. 2.2), information about the cumulus parameterizations and model resolution (Sect. 2.3), and
137   analysis methods in Sect. 2.4. A description of the case study is found in Sect. 2.5. The results are outlined in Sect.
138   3, with a discussion on the temporal evolution of dust concentrations and dust uplift potential in Sect. 3.1, vertical

139 distributions and fluxes of dust in Sect. 3.2, and the effect on aerosol radiative heating rates in Sect. 3.3. A

140 discussion of the results and implications for the community are located in Sect. 4 and a summary of the findings of

141 this study are reviewed in Sect. 5.

142 **2) Case study and model description**

143 **2.1) WRF-Chem model description and physics**

144 To investigate the Arabian Peninsula case study, WRF-Chem version 3.9.1.1 was used to simulate the dust outbreak

145 meteorology and aerosol fields. WRF-Chem is an online numerical chemical transport model that allows for

146 interactive aerosol processes, including feedbacks between the meteorology, aerosol, and radiation. The model was

147 coupled to the Goddard Chemistry Aerosol Radiation and Transport (GOCART) module (Ginoux et al., 2001),

148 which allowed for feedbacks between the meteorology and aerosols and is described in more detail in Sect. 2.2. The

149 model was tested with and without dust initial and boundary conditions from the Community Atmosphere Model

150 with Chemistry (CAM-Chem) global model (Emmons et al. 2010). The concentrations of dust advected through the

151 lateral boundary conditions was too small to have an effect on the results, and the initial conditions introduced a

152 spurious decreasing integrated dust trend over time when modeled aerosol optical depth (AOD) was compared to

153 AERONET observations. While the initial conditions led to a higher integrated dust mass, it did not change the

154 conclusions of the study. To remove this factor and focus more on the meteorological processes that actively loft and

155 transport dust in real-time, no chemistry or aerosol initial / lateral boundary conditions were used. Rather, the

156 aerosol fields were initialized with zero concentrations and were allowed to evolve naturally from the model

157 meteorology, aerosol, surface and radiation processes.

158

159 The meteorological and sea surface temperature initial and lateral boundary conditions were sourced from the 0.25

160 degree, 6-hourly Global Data Assimilation System Final Analysis (GDAS-FNL). The model was run from 00:00:00

161 UTC on 02-Aug-2016 to 00:00:00 UTC on 05-Aug-2016 producing output at 30-minute intervals. The following

162 model parameterizations were employed and kept constant across the simulations, with similar WRF physics options

163 being utilized elsewhere to study dust effects (e.g. Alizadeh Choobari et al. 2013): Morrison double-moment

164 microphysics (Morrison et al., 2005; 2009), RRTMG longwave scheme (Iacano et al., 2008), Goddard shortwave

165 radiation scheme (Chou and Suarez, 1999), the Noah Land Surface Model with multiparameterization options (Niu

166 et al., 2011; Yang et al., 2011), and the MYNN level 3 boundary layer parameterization (Nakanishi and Niino, 2006;

167 2009). The convective parameterizations and horizontal resolutions tested will be discussed in Sect. 2.4. A summary

168 of the physics options utilized can be found in Table 1.

169

170 **2.2) GOCART dust emissions and dust uplift potential**

171 WRF-Chem is coupled to the GOCART dust module, which parameterizes the emission of dry mineral dust mass

172 from the surface. GOCART is single-moment in mass, meaning there is no number information available to change

173   the number of cloud condensation nuclei or ice nuclei in the microphysics. As such, the indirect effects of dust

174   cannot be simulated with this setup. Through this model, dust is emitted to the atmosphere in 5 discrete effective

175   radii bins [0.5, 1.4, 2.4, 4.5, and 8.0 μm] based on Eq. (1):

176     $F_p = CSs_p U^2 (U - U_t) \ if \ U > U_t$ (1)

177   In Eq. (1), F_p is the dust flux from the surface [kg m^{-2} s^{-1}] for each of the radii bins (p), S represents the wind erosion

178   scaling factor [0 to 1] established by the Ginoux et al. (2004) soil erodibility map, s_p is the fraction of each size class

179   within the soil [0 to 1] based on the silt and clay fraction of the soil type, U is the 10 m wind speed [m s^{-1}], and U_t is

180   the threshold velocity of wind erosion [m s^{-1}]. C is a tuning constant (set here to a default 1 kg s^2 m^{-5}), which can be

181   set by the user to increase or decrease the total dust flux based on regional observations (e.g. Zhao et al., 2010;

182   Kalenderski et al., 2013; Dipu et al., 2013). If the wind speed is less than the threshold velocity, no dust will loft

183   from the surface. Most of the terms in Eq. (1) are time invariant (C,S,s_p), except for the wind speed (U) and wind

184   erosion threshold (U_t). U_t is a function of soil wetness, and is calculated with the relationship found in Eq. (2):

185     $U_t = \begin{cases} 6.5\sqrt{\frac{\rho_p - \rho_a}{\rho_a} g D_p}(1.2 + log_{10} w_{soil}) & if \ w_{soil} < 0.5 \\ \infty & if \ w_{soil} \geq 0.5 \end{cases}$ (2)

186   For Eq. (2), ρ_p is the dust particle density [kg m^{-3}], ρ_a is the density of air [kg m^{-3}], g is gravitational acceleration [m

187   s^{-2}], and w_{soil} is the soil wetness fraction [0 to 1]. Similar to Eq. (1), Eq. (2) includes a threshold, whereby above a

188   soil wetness of 0.5, no dust will be emitted. If the threshold criteria are met and dust lofts from the surface, it is then

189   transported based on the simulated meteorological fields from WRF, including advection, convection, and turbulent

190   mixing, and is removed from the atmosphere via gravitational settling and wet deposition. Here, wet deposition is

191   included as a scavenging mechanism to provide a more realistic picture of the moist convection transport process.

192   Aerosol radiation interactions in the shortwave and longwave (Barnard et al., 2010) are included in the simulations

193   to understand the implications that lofted dust has on the energy budget of the case study and are discussed in Sect.

194   3.3.

195   Before dust can amass in and influence the atmosphere, it must first be emitted from the surface. Because of the

196   threshold values included in the GOCART dust parameterization equations (Eq. 1-2), it is important to understand

197   how often the modeled near-surface wind speeds exceed the wind threshold value. A parameter useful in describing

198   the influence of the wind on dust emissions is Dust Uplift Potential (DUP), proposed by Marsham et al. (2011) and

199   based on Marticorena and Bergametti (1995). The DUP parameter is an offline approximation for the relative

200   amount of dust expected to loft from the surface. DUP is a convenient way to perform first order sensitivity tests on

201   the meteorology without having to re-run the model, and provides a framework for deconvolving the variables in Eq.

202   (1-2). Here, we have adapted the DUP parameter from Marsham et al. (2011) (Eq. 4) into three variations (Eq. 3-5),

203   which allows researchers to vary the complexity of the analysis by including more, or fewer degrees of freedom.

204     $DUP(U) = U^3 \left(1 + \frac{A}{U}\right)\left(1 - \frac{A^2}{U^2}\right)$ (3)

205 $$DUP(U, U_t) = U^3 \left(1 + \frac{U_t}{U}\right)\left(1 - \frac{U_t^2}{U^2}\right)$$ (4)

206 $$DUP(U, U_t, S) = SU^3 \left(1 + \frac{U_t}{U}\right)\left(1 - \frac{U_t^2}{U^2}\right)$$ (5)

207 In Eq. (3), U_t is set to a constant wind speed, A, thereby making DUP a function of only the near-surface wind

208 speed; for the purpose of this paper U_t is set to 5 m s^{-1}, but has been tested elsewhere across the range of 5-10 m s^{-1}

209 (e.g. Marsham et al., 2011; Cowie et al., 2015; Pantillon et al., 2015). This simplified equation for dust uplift has

210 been used in previous dust studies, and is useful to include here to place this manuscript in the context of existing

211 literature. Eq. (4) is slightly more intricate in that it considers the model evolution of U_t due to changing soil wetness

212 from precipitation and land-surface processes, calculated by Eq. (2). Lastly, Eq. (5) builds on Eq. (4) by including

213 the soil erodibility scaling factor (S), which recognizes that the U and U_t relationship is valid only if it occurs over

214 potential dust source regions. Since U, U_t, and S are entangled in the GOCART dust parametrization found in Eq.

215 (1-2), the seemingly minor variations between the DUP parameters in Eq. (3-5) are crucial for isolating which

216 processes, or combination of processes, are sensitive to the horizontal resolution of the model, and hence to the

217 analysis performed here.

218 **2.3) Domain, nesting, and cumulus parameterizations**

219 Several horizontal model grid-spacings (45 km, 15 km, and 3 km) of the Arabian Peninsula domain (Fig. 3) were

220 tested to identify the sensitivity of modeled dust concentrations to the model's horizontal resolution. For the two

221 coarsest simulations (45 km and 15 km), cumulus parameterizations were employed to represent shallow and deep

222 convection. The 45 km simulation was run with only the Betts–Miller–Janjic (BMJ) cumulus parameterization

223 (Janjic, 1994), while five different cumulus parameterizations were tested for the 15 km simulations, including the

224 BMJ, Kain–Fritsch (KF) (Kain, 2004), Grell 3D Ensemble (GD) (Grell, 1993; Grell et al., 2002), Tiedtke (TD)

225 (Tiedtke, 1989; Zhang et al., 2011), and Simplified Arakawa–Schubert (AS) (Arakawa and Schubert, 1974; Han and

226 Pan, 2011) schemes, which will determine the sensitivity of dust lofting to different cumulus parameterizations. A

227 15 km simulation with no cumulus parameterization was also run, but the results were similar and within the spread

228 of the 15 km simulations that employed cumulus parameterizations and are not included here. The finest resolution

229 simulation (3 km) was run at convection-permitting scales and hence no cumulus parameterizations were invoked.

230 The 3 km simulation was initialized as a one-way nest from the 15 km BMJ simulation, which served as its parent

231 lateral boundary conditions. Other combinations of nests were tested, but the results were not sensitive to which 15

232 km simulation was used as the parent nest, or lateral boundary conditions, for the 3 km simulation. A summary of

233 the model domains is also found in Fig. 3.

234 The cumulus parameterizations tested in this study for the 15 km simulations vary in their methods for triggering

235 and then characterizing convective processes at the sub-grid scale level. BMJ is a moisture and temperature

236 adjustment scheme that acts to restore the pre-convective unstable thermodynamic profile to a post-convective stable

237 and well-mixed reference profile, while the other cumulus parameterizations (KF, GD, TD, AS) employ a mass-flux

238 approach to determine updraft and downdraft mass transport. Across the mass-flux parameterizations, GD is unique

239   in that it computes an ensemble of varying convective triggers and closure assumptions and then feeds the ensemble

240   mean back to the model. Furthermore, all five schemes represent shallow convection in addition to deep convection,

241   the mass-flux schemes include detrainment of water and ice at cloud top, and AS and TD are formulated to include

242   momentum transport in their calculations. These differences across parameterizations will result in varying updraft

243   and downdraft speeds and precipitation rates, which will have consequences for the vertical transport of airborne

244   dust, as well as the strength of convective outflow boundaries and therefore dust emission at the surface. Several

245   cumulus parameterization schemes were tested to introduce spread into the solutions and to represent the 15 km

246   results as a 5-member ensemble mean with uncertainty estimates. Because this paper seeks to investigate the effect

247   of horizontal resolution on dust transport, comparing individual cumulus schemes against one another is outside the

248   scope of this study.

249   **2.4) Averaging and analysis methods**

250   Because the representation of convective processes varies across the simulations, the results will focus on composite

251   statistics from the three-day case study. The authors make no attempt to track and match individual convective

252   elements across simulations, as their triggering, timing, and development (or lack of development) will fluctuate

253   depending on the model resolution and cumulus parameterization, thus making a truly consistent analysis

254   problematic. Instead, this paper takes a step backward and aims to quantify in an average sense, how the choice of

255   horizontal resolution and parameterized convection affects dust concentrations in the WRF-Chem model across the

256   Arabian Peninsula. The analyses and averages are processed within the yellow box shown in Fig. 3, disregarding all

257   other grid points outside the Arabian Peninsula study area. Analyses that are averaged in time are only averaged

258   over the last two days of the simulation (00:00:00 UTC on 03-Aug-2016 to 00:00:00 UTC on 05-Aug-2016) to

259   account for model spin up in the first 24 hours. All results are summed over the five dust bins in the GOCART

260   model rather than being treated separately. Lastly, the results from the five 15 km simulations are averaged together

261   to produce a mean 15 km resolution response, and is presented, along with the maximum and minimum spread

262   across these simulations for reference.

263   **2.5) Case study overview**

264   The dust event simulated for this study occurred during August 2-5, 2016 across the Arabian Peninsula, originating

265   from a combination of synoptic and mesoscale dust sources. A meteorological analysis of this event, including an

266   attribution of specific dust sources to meteorological features can be found in Miller et al. (2019) and will not be

267   reiterated in detail here. Rather, a snapshot of the meteorology and dust fields from the WRF-Chem simulation on

268   August 3rd at 15:00:00 UTC can be found in Fig. 1-2 as a reference to the typical meteorological setup for this case

269   study.

270   For this event, the high summertime temperatures in the desert of the Arabian Peninsula produce a thermal low

271   couplet at the surface, with one low centered over Iraq and the other over the Rub' al Khali desert in Saudi Arabia

272   (Fig. 1.c). The local low-pressure couplet leads to cyclonic surface winds between these two areas (Fig. 1.e),

273   comprised of northerly flow from Iraq into Saudi Arabia, with retuning southerly flow from Oman over the Persian

274 Gulf and into Kuwait, and is a major non-convective contributor to the dust budget for this case study (Fig. 1.f). In
275 addition to these large-scale flow patterns, a daytime sea breeze brings moist, maritime air from the coast of Yemen
276 and Oman inland into the otherwise arid Saudi Arabian basin (Fig. 1.e and 1.d). This moisture gradient is also
277 evident in the skew-t diagrams, which represent an inland radiosonde release site at Riyadh (Fig. 2.a), and a site
278 closer to the coast in Abha (Fig. 2.b), both located in Saudi Arabia. There is a stark difference in low-level moisture
279 between the two sites, although both display a subsidence inversion aloft between 500 and 600 hPa. Furthermore,
280 nocturnal low-level jets form along the Zagros mountains in Iran and Iraq, and the Red sea, both of which have been
281 studied previously in the literature (Giannakopoulou and Toumi, 2011; Kalenderski and Stenchikov, 2016).

282 Due to the region's inherent moisture constraints, convection is limited spatially to the coastal regions of the
283 Arabian Peninsula, as is most summertime convective and non-convective precipitation in this region (e.g. Shwehdi,
284 2005; Almazroui, 2011; Hasanean and Almazroui, 2015; Babu et al., 2016). Moist convective cells develop along a
285 low-level convergence line between the northerly basin flow and sea breeze front (Fig. 1.g and 1.h) aided by
286 elevated terrain in Yemen and Oman (Fig. 1.a). This convective setup along the southern portion of the Arabian
287 Peninsula is a feature evident in each day of this case study, initializing diurnally in the local late afternoon and early
288 evening, and thereby providing three days of data for analysis, with the height of convective activity occurring on
289 August 3rd. Individual convective cells form along the convergence line, a typical Middle Eastern characteristic
290 (Dayan et al., 2001), but do not organize further, owing to a lack of upper-level synoptic support and insufficient
291 moisture in the interior of the peninsula. Nevertheless, the convective line does produce outflow boundaries, which
292 loft dust from the surface and are the main convective dust source for this case study. More information on model
293 validation of this study, including comparisons of these simulations with AOD observations can be found in Saleeby
294 et al. (2019), which shows that WRF-Chem systematically underestimates dust AOD for this event.

295 **3) Results**

296 **3.1) Temporal evolution**

297 **3.1.1) Dust uplift potential**

298 The first process of interest in determining the sensitivity of modeled dust concentrations to horizontal resolution in
299 WRF-Chem is the amount of dust lofted from the surface to the atmosphere. Fig. 4 depicts the average DUP for the
300 simulations at each 30-minute output, using Eq. (3-5) to separate out the importance of the different mechanisms
301 regulating dust emissions.

302 Regardless of which DUP parameter is used, almost all of the simulations capture the bimodal daily maximum in
303 dust emissions in the local mid-morning (6 UTC) and late afternoon (13 UTC) due to the mixing of the NLLJ to the
304 surface and convective outflow boundaries, respectively. The only resolution where the bimodality is absent is the
305 45 km simulation, which captures the NLLJ mechanism, but misses the second convective activity maximum. The
306 coarsest simulation overestimates the near-surface wind speeds related to the NLLJ mechanism, which subsequently

307 inhibits convection later in the day. Because of this, the 45 km simulation has the highest DUP(U) (Fig. 4.a) based

308 only on wind speed (Eq. 3), a result similar to the Heinhold et al. (2013) and Marsham et al. (2011) studies over the

309 Sahara.

310 However, when taking the calculated threshold wind velocity into account (Eq. 4), the convection-allowing

311 simulation (3 km) displays the strongest DUP(U,U$_t$) at the local late afternoon convective maximum (Fig. 4.c). For

312 this to be the case compared to the DUP(U) parameter, the 3 km simulation must have a lower threshold wind

313 velocity (Fig. 5.a) than the simulations with parameterized convection. Since the threshold wind velocity is

314 proportional to soil wetness (Eq. 2), this implies that the convection-permitting simulation will on average have drier

315 soil, or more grid points below the soil wetness threshold than the parameterized simulations. Rainfall is generated

316 differently in parameterized versus convection-allowing simulations, and it has been well documented that

317 parameterized simulations produce more widespread light rainfall, whereas more intense rainfall tends to develop

318 over smaller areas in convection-allowing simulations (e.g. Sun et al., 2006; Stephens et al., 2010). From a domain

319 average perspective, rainfall in the 3 km simulation will cover less area, leading to the soil moisture threshold not

320 being exceeded as frequently compared to the parameterized cases.

321 This spatial difference in rainfall leads to the 3 km case having drier soil on average across the domain, which is

322 evident in the surface fluxes represented by the Bowen ratio of sensible to latent heat fluxes in Fig. 5.c. When the

323 Bowen ratio is above one, more of the surface heat exchange with the atmosphere is in the form of sensible heat

324 flux, rather than latent heat flux. Dry soils are characterized by low values of latent heat flux, and therefore exhibit

325 higher Bowen ratios. The 3 km simulation exhibits a higher Bowen ratio on August 3rd and 4th, indicating that the

326 soil is on average drier in the convection-permitting simulation. This result implies that disparities in land surface

327 properties across the varying model grid resolutions are important for modulating dust emissions, both from the

328 perspective of convection-allowing versus parameterized convection and associated precipitation, as well as latent

329 and sensible heat fluxes.

330 Adding on to the complexity of the DUP parameter, when the location of dust sources is considered in the

331 DUP(U,U$_t$,S) calculations (Eq. 5), some of variability between the local NLLJ and convection maxima is lost in the

332 3 km simulation (Fig. 4.e) on August 3rd. Also, including the scaling factor reduces the magnitude of the DUP

333 parameter to roughly 10% of the initial values for DUP(U) and DUP(U,U$_t$). Incorporating the dust source function in

334 DUP works not only as a scaling factor for the magnitude of potential dust emissions, but also impacts the relative

335 importance of dust production mechanisms (NLLJ versus convection). This shift is a consequence of the location in

336 which these processes occur. For instance, the reduction in the 3 km convective maximum on August 3rd between

337 DUP(U,U$_t$) and DUP(U,U$_t$,S) signifies that convection is occurring in locations that are not active dust source

338 regions. Without information on the dust source regions, this process would be assigned an unrealistic dominance

339 over the NLLJ mechanism in terms of DUP.

340 All simulations are similar for the first 24 spin-up hours until the processes begin to diverge on August 3rd, where

341 the convection-allowing simulation produces the maximum DUP(U,U$_t$,S) both during the local daytime and

342   nighttime hours. On the final day of the case study (August 4th), the convection-allowing simulation has the lowest

343   DUP(U,U_t,S), with the NLLJ maximum dominating over the convective maximum in both the 3 km and the 15 km

344   mean, due to reduced convective activity in the fine resolution simulations. Examining the percent difference in

345   DUP between the coarse and fine simulations (Fig. 4.b,d,f), the average percent difference between the 3 km and 15

346   km simulations is at a minimum when only wind speed is considered, and increases as the degrees of freedom in

347   DUP increases. For the DUP(U,U_t,S) case, the average percent difference is between 10-65% lower in the 15 km

348   simulations than the convection-permitting simulation, with a maximum difference of 85% and a spread across

349   parameterizations of 20%. This implies that the convection-allowing WRF-Chem simulation has the potential to loft

350   up to 85% more dust than those with parameterized convection.

351   **3.1.2) Vertically integrated dust mass**

352   The differences in DUP(U,U_t,S), or dust flux from the surface to the atmosphere, specifically the enhanced values

353   for the convection-permitting simulation on August 3rd, will lead to more dust lofting than in the coarse simulations.

354   To see how differences in the dust emissions translate into differences in airborne concentrations of dust, Fig. 6

355   demonstrates the temporal evolution of the spatially averaged, vertically integrated dust mass throughout the vertical

356   column. Here, the convection-allowing simulation records upwards of 150% more integrated dust mass compared to

357   the coarse resolution simulations. Across the coarse simulations, the 45 km and 15 km runs have similar vertically

358   integrated dust magnitudes, despite the temporal differences in DUP(U,U_t,S). This is due to the overestimation of

359   the NLLJ in the 45 km simulations being offset by the enhanced convective dust lofting in the 15 km simulations.

360   The discrepancy in the diurnal maxima across horizontal resolutions is similar to the results of the UM in Marsham

361   et al. (2011) and Heinhold et al. (2013). Yet, the results here differ in that both of these previous studies found a

362   stronger NLLJ response in 12 km simulations with convective parameterizations than was found here in the 15 km

363   parameterized ensemble. In contrast to the findings of Marsham et al. (2011) and Heinhold et al. (2013), dust

364   emissions and airborne dust mass increases in the WRF-Chem simulations in the convection-allowing simulation,

365   which is in closer agreement to the studies of Reinfried et al. (2009) and Bouet et al. (2012) who used COSMO-

366   MUSCAT and RAMS-DPM respectively. Considering each study used a different model and therefore physics, it is

367   unsurprising that the results vary. However, it is not apparent how much of a role the region or specific case study

368   plays in this difference and is an area for future work.

369   The temporal trends in vertically integrated dust mass lag behind those observed in the DUP plots in Fig. 4.

370   Particularly at timesteps where DUP decreases, the change in integrated dust mass follows several hours later. The

371   time series of gravitational settling rates at the surface (Fig. 5.b) also lags behind the DUP trends, which implies that

372   the removal mechanisms for dust take time to act on the airborne particles once they are emitted. The rates of

373   gravitational settling are higher in the convection-permitting simulation compared to the coarse simulations because

374   more dust is available aloft to settle out. Nevertheless, Fig. 6.a suggests that this increase in gravitational settling

375   rates in the 3 km case is not enough to offset the higher dust emissions, or the vertically integrated dust quantities

376   would be similar across all the simulations. The fact that the vertically integrated dust values are higher in the 3 km

377 simulation, despite higher rates of gravitational settling, implies there must be a mechanism that acts to keep dust

378 suspended longer in the convection-permitting simulations than in those with parameterized convection. There are

379 clearly more processes occurring above the surface to influence the vertically integrated dust quantities than just a

380 simple surface emission to surface deposition ratio. This will be further deconstructed by examining vertical profiles

381 in the following section.

3.2) Vertical characteristics

3.2.1) Vertical dust and velocity profiles

384 Moving away from vertically integrated quantities to a time and domain averaged vertical snapshot of dust (Fig.

385 7.a), the vertical dust profile follows a generally exponentially decreasing function and tapers off to low dust

386 concentrations in the range of 5-6 km above ground level (AGL). A widespread subsidence inversion is present near

387 6 km throughout the case study time period over the inner basin of the Arabian Peninsula (Fig 2), acting as a cap on

388 vertical motions and dust transport. Because dust concentrations do not vary much above this height, the plots in

389 Fig. 7 have been truncated at 9 km. There is a higher concentration of dust at every level in the convection-allowing

390 simulation compared to that in the coarse simulations. Examining the percent difference plot between the

391 convection-permitting and other simulations in Fig. 7.b, there is a difference of approximately 80% at the surface,

392 which increases upwards to ~180% at 6 km. Above this level, the percent difference between the convection-

393 permitting and coarse simulations changes sign, but the overall concentration is extremely low, and as such, the

394 authors make no attempt to assign meaning to the differences above 6 km.

395 For dust to reach higher levels in the atmosphere, it must have undergone vertical transport to move it aloft from its

396 initial source region at the surface. Several mechanisms could be responsible for vertical dust transport in the

397 Arabian Peninsula, including flow over terrain, daytime mixing (dry convection), and lastly, moist convective

398 updrafts, whose representation (explicit versus parameterized) is a defining difference between the horizontal

399 resolutions tested in this paper. Investigating the effect that increasing resolution has on updraft and downdraft

400 strength can be found in Fig. 8, which represents the mean of all vertical velocities above or below 0 m s^{-1}, including

401 points that are not vertically continuous. As resolution increases, the average range in vertical velocity also

402 increases. The simulations with parametrized convection have lower mean updraft / downdraft speeds than the

403 convection-allowing simulation, on the order ~75% weaker near the surface for the 15 km runs and ~110% weaker

404 for the 45 km run. It is known that in numerical models, the updraft radius scales with the grid spacing (e.g. Bryan

405 and Morrison, 2012), with a compensating increase in updraft speed as the radius decreases. This relationship skews

406 the frequency of vertical velocities to higher values. Irrespective of resolution, the mean updraft speeds in the WRF-

407 Chem simulations are slightly higher than the downdraft speeds, while at the surface mean downdraft speeds are

408 higher than updraft speeds, a consideration that will be discussed further in Sect. 3.2.2.

3.2.2) Vertical dust flux

The implication for dust transport based on vertical velocities is convoluted, since updrafts and downdrafts work concurrently to redistribute aerosol. As noted in Jung et al. (2005), convective updrafts will lift aerosol particles upward into the free atmosphere, while downdrafts simultaneously limit the maximum vertical extent of these particles. However, the convective transport simulations in Jung et al. (2005) demonstrate that these opposing processes do not act as equal opposites in time, magnitude, and space. This canon holds true for the Arabian Peninsula simulations as well. Fig. 9 contains Contoured Frequency by Altitude Diagrams (CFADs) of vertical velocity (Yuter and Houze, 1995) normalized by the total number of grid points in each simulation. The normalization is performed to remove an artificial larger frequency in the higher resolution simulations that arises because there are more grid spaces available to count. Because no vertical velocity threshold is imposed, a majority of points straddle zero. To highlight variability away from the zero line, the CFAD contours are plotted on a log scale.

Similar to the mean plots in Fig. 8, as resolution increases, so does the variability in updraft and downdraft speeds. There is a striking difference between the spread in vertical velocities at all altitudes across the 45 km, 15 km mean, and 3 km simulations in Fig. 9. In the 45 km run, most of the velocities straddle +/- 1-2 m s^{-1}, whereas the convection-permitting simulation ranges from -10 to 30 m s^{-1}. Not only is the range larger, but the normalized frequency is greater in the fine resolution simulation as well. The inference here is that stronger updrafts will transport dust higher in the atmosphere, and that stronger updrafts are observed more frequently in the convection-allowing simulation, thereby enhancing the vertical dust transport.

Combining the information on the vertical distribution of dust and updraft / downdraft speeds, it is possible to calculate a domain averaged dust flux profile (Fig. 8). Again, the magnitude of the dust flux upwards and downwards from the surface through 6 km AGL is higher in the convection-allowing simulation compared to the parametrized simulations. Moreover, the mean near-surface upwards dust flux is stronger than that for the downward dust flux, which coincides with the mean updraft speeds being slightly higher than the mean downdraft speeds at these same vertical levels (Fig. 8). This relationship also holds in the dust flux CFADs (Fig. 9), in which the upward and downward flux of dust has more variability in the 3 km simulation, and stronger vertical dust fluxes are more frequent.

Similarly, there is more dust transport evident at higher vertical levels in the convection-permitting simulation, which has implications for the residence time of the dust particles. As dust is transported higher in the atmosphere, absent any sort of external motion or coagulation outside of gravitational settling, the atmospheric lifetime of the particles will increase. Figure 10 shows the theoretical terminal velocity of dust particles in WRF-Chem using the Stokes settling velocity with slip correction for pressure dependence (Fig. 10.a) and their lifetime based on different starting heights in the atmosphere (Fig. 10.b), which increases exponentially away from the surface. As such, dust in the convection-permitting simulation will take longer to settle out, leading to the higher observed vertically integrated dust values (Fig. 5) compared to the parameterized simulations. Looking at the distribution of downdrafts

444   in the vertical velocity CFADs (Fig. 9), there is a clear bimodal signal aloft in both the convection-permitting and 15

445   km simulations, being representative of two distinct subsidence layers, which act as a cap on vertical transport. The

446   local minimum occurs around 6 km, which could explain why dust fluxes also taper off at this level.

447   At the surface, higher dust flux values are found in association with the downdrafts, producing a pronounced

448   skewness towards high, yet infrequent values of strong negative dust flux towards the ground (Fig. 9). It is

449   hypothesized that this skewness is a consequence of the dissimilar background dust conditions in the vicinity of

450   near-surface downdrafts and updrafts, similar to the results found in Siegel and van den Heever (2012), which

451   studied the ingestion of dust by a supercell storm. Updrafts originate in relatively clear air, and will consume

452   background dust and transport it upwards. However, downdrafts occur through the cold pool, and hence their source

453   is, at least partially, within the dusty cold pool. As such, downdrafts will have access to more dust and thus transport

454   more of it in the downward direction. This skewness warrants further research, preferably from an idealized

455   perspective, to better understand the relationship between storm dynamics, dust emissions, and transport.

456   In all, the increased vertical dust concentration profile and vertically integrated dust values in the 3 km run are a

457   product of several processes working together. Compared to the simulations with parameterized convection, the 3

458   km run has enhanced potential for dust uplift due to stronger resolved downdrafts and lower wind velocity

459   thresholds, higher vertical transport due to more frequent, stronger updrafts, and a lengthier theoretical residence

460   time once being lofted to higher levels.

461   **3.3) Impacts on radiation**

462   Beyond the first-order sensitivity of model resolution to dust emissions and concentrations for the Arabian Peninsula

463   case study, there are higher-order effects that disseminate from changing dust concentrations. One example being

464   the modification of atmospheric heating / cooling rates and the radiation budget due to dust absorption and scattering

465   (see Sect. 1). The domain and time averaged shortwave (SW), longwave (LW), and net dust heating / cooling rates

466   are found in Fig. 11. The average dust heating and cooling rates were calculated over the last 48 hours of the

467   simulation as a difference between the radiation tendency with dust aerosols and without. Ostensibly, since dust

468   concentrations increase in the model as resolution increases, so does the magnitude of the radiative effects. There is

469   a stronger SW cooling and LW heating effect in the 3 km simulation, and this trend follows the vertical distribution

470   of dust from Fig. 7, again tapering off near 5-6 km AGL.

471   Most interestingly, however, is the difference in the net aerosol heating rate. In the lowest layer (<1.5 km), there is a

472   sign change between the fine and coarse simulations. The SW effect in the convection-allowing simulation is strong

473   enough to elicit a net cooling effect in this near-surface layer. Conversely, the LW aerosol heating effect dominates

474   in the coarse simulations, resulting in a net warming effect. The model has a stronger shortwave effect for dust based

475   on the prescribed index of refraction, but is also related to the timing of dust emissions, considering the SW effect is

476   only active during the daytime. The difference between warming and cooling can have cascading effects on the

477   thermodynamic profile, static stability, and future convective development, which in turn impacts the relative

478   importance between convection and the NLLJ discussed earlier. The sensitivity of dust concentrations to horizontal

479   model resolution is important to understand in its own right, but furthermore, this sensitivity leads to higher-order

480   changes in model predictions. If NWP models or GCMs are going to incorporate dust radiative effects,

481   concentrations need to be highly constrained, not only to accurately capture the magnitude, but the sign of the

482   response as well.

483   **4) Discussion and recommendations**

484   For this Arabian Peninsula event, horizontal resolution in the WRF-Chem model has a considerable effect on the

485   dust budget of the region. Because aerosol prediction models and GCMs still employ cumulus parameterizations, it

486   is important to discuss the uncertainties unearthed in this paper, as well as recommendations for past and future

487   forecasts and research that will be generated prior to our ability to consistently run these models at convection-

488   permitting resolutions.

489   In an average sense, there will be higher dust concentrations produced in convection-permitting simulations

490   compared to those with parameterized convection. The major point here is that the uncertainty in dust concentrations

491   for simulations using different cumulus parameterizations (15 km ensemble), or using different horizontal

492   resolutions with the same cumulus parameterizations (45 km versus 15 km) is small relative to the differences

493   between the use of parameterized versus convection-allowing scales. *Most of the uncertainty in the model's*

494   *predicted dust concentrations comes from the choice to either parameterize convection or run at convection-*

495   *permitting scales.*

496   The results of this research do not stand alone in the literature focused on the impact of horizontal model resolution

497   on dust emissions, and there are several similarities and differences to note when comparing this paper to previous

498   studies. Firstly, concerning the diurnal variation in dust emissions, we find a similar response in the NLLJ

499   mechanism to that of Heinhold et al. (2013) and Marsham et al. (2011), whereby the coarsest simulations

500   overestimate the early morning windspeeds caused by the mixing of the jet to the surface and fail to capture the late

501   afternoon / early evening convective dust lofting mechanism. In these previous studies, the convection-allowing

502   simulation reduces the importance of the NLLJ and enhances the convective maximum, but still retains the NLLJ as

503   the dominant process for dust uplift. Overall, Heinhold et al. (2013) and Marsham et al. (2011) found a net reduction

504   in dust uplift while running at convection-permitting scales. While the NLLJ mechanism is found to be similar here,

505   the analysis reveals an opposite response in WRF-Chem for the Arabian Peninsula, in which the convective

506   maximum dominates, but the NLLJ is still an important mechanism, which thereby leads to more, rather than less

507   dust in the convection-allowing simulations. The net increase in dust concentrations in WRF-Chem is similar to the

508   findings of Reinfried et al. (2009), although Reinfried et al. (2009) focused mainly on haboobs, which may point to

509   convection being the source of agreement rather than the balance between the NLLJ and convection. At this point,

510   we cannot determine whether the discrepancies between our results and previous literature comes from regional or

511   case study differences in the importance of these mechanisms to the dust budget, differences in the models'

512   representation of these processes, or a combination of the two. In all, more work needs to be done to investigate the

513   relationship between the NLLJ and subsequent late afternoon convection in dust producing regions, and the

514   representation of this in numerical models.

515   From a vertically integrated viewpoint, for the Arabian Peninsula region it is possible to rudimentarily tune the dust

516   concentrations of the coarse simulations to that of the convection-permitting simulation by multiplying by an

517   average constant derived from the dust difference plots in Fig. 6-7, which would be on the order of ~2. This is an

518   offline solution, which would aid in enhancing the accuracy of a first-order forecast of vertically integrated or

519   surface dust, and/or AOD. This factor would have to be scaled further, since comparison of the WRF-Chem model

520   to AERONET sites and other AOD observations (Saleeby et al. 2019) shows that WRF-Chem underestimates dust

521   under these conditions. Nevertheless, attempting to use this tuning parameter online in the model (i.e. adjusting the

522   tuning constant, C, in Eq. 1) would not reconcile the differences from a dust flux standpoint. Even if more dust were

523   to be emitted from the surface, the parameterized simulations still lack the necessary variability in updrafts and

524   downdrafts, especially updraft strength, to transport the dust upwards and away from the surface, thus

525   misrepresenting the atmospheric lifetime of these particles in the process.

526   Moreover, tuning the dust concentrations will not change the effect horizontal resolution has on the soil

527   characteristics, particularly soil moisture, and hence on the a priori determined threshold wind speeds which are

528   important in calculating dust lofting in the first place (Fig. 4). If dust concentrations are inaccurately predicted in the

529   coarse simulations, or erroneously tuned, the higher-order online feedbacks will also be incorrect, such as

530   modifications to the radiative budget, and feedbacks to the thermodynamic profile, static stability and mesoscale

531   features, particularly those driven by differences in thermodynamic gradients, such as sea breezes and cold pool

532   propagation.

533   **5) Conclusions**

534   In this study, we have quantified the response sign and magnitude in modeled dust fields in the WRF-Chem regional

535   model to increasing horizontal resolution and the manner in which convection is represented for a summertime

536   Arabian Peninsula event. We have investigated the variability in dust concentrations and fluxes due to the choice of

537   convective parameterization, the representation of convection in the model (explicit versus parameterized), and the

538   effect these differences in dust concentrations have on aerosol heating rates. The case study was simulated at three

539   different horizontal resolutions (45 km, 15 km, and 3 km), with the two coarsest simulations run with cumulus

540   parameterizations, and the 3 km simulation run at convection-permitting resolution. To understand the uncertainty

541   across different parameterizations, five separate cumulus parameterizations were tested in an ensemble (BMJ, AS,

542   GD, TD, KF) at 15 km grid spacing.

543   The convection-allowing simulation exhibited a stronger potential for dust uplift as a function of modeled wind

544   speed, wind threshold, and the location of dust sources. The wind threshold for dust lofting in the 3 km simulation

545   was on average, lower than that for the 15 km or 45 km. This is due to differences in grid resolution leading to

546 changes in the soil moisture, whereby the 3 km simulation displays lower soil wetness across the domain.
547 Furthermore, a distinct difference across simulations was identified in the representation of the bimodal daily
548 maximum in dust emissions in the local mid-morning (mixing of the NLLJ to the surface) and late afternoon
549 (convective outflow boundaries). Compared to the 3 km case, the 45 km simulation overestimates the contribution
550 from the NLLJ and underestimates the role of convection in dust emissions.

551 The 3 km simulation also produced higher vertically integrated dust values at every timestep, as well as higher dust
552 concentrations at every vertical level in the lower troposphere (below 6 km AGL). The uncertainty in dust
553 concentrations for simulations using different cumulus parameterizations (15 km ensemble spread) is much smaller
554 than the difference between the parameterized and convection-permitting convection cases. For the WRF-Chem
555 Arabian Peninsula simulations, the modeled dust fields were most sensitive to the choice of parametrizing or
556 explicitly resolving convective processes. The enhanced dust concentrations in the convection-allowing case are the
557 result of stronger downdrafts lofting more dust from the surface, and stronger updrafts carrying dust to higher levels
558 of the atmosphere, thereby increasing the airborne lifetime of the dust particles. The difference in dust mass across
559 the simulations leads to a significant modification of the radiation budget, specifically the aerosol heating rate. The
560 convection-allowing simulation revealed a greater shortwave and longwave effect, and for aerosol heating rates in
561 the lowest levels, shortwave cooling is stronger than longwave heating, leading to a net cooling effect. Conversely,
562 the opposite radiative response is present in the parameterized cases, resulting in a net warming effect, causing a
563 change in sign in the lowest levels compared to the convection-permitting case.

564 There are a number of implications these results may have on forecasting and future studies. The dust concentrations
565 in the coarse simulations could be tuned offline to match those in the convection-allowing simulation using the
566 percentage difference plots included in Fig. 5-6. This tuning would be on the order of ~2. However, because vertical
567 transport is essential to the vertical concentrations and lifetime of the particles, this tuning factor cannot be applied
568 online. Even if such a tuning were applied, this change will not accurately capture higher-order feedbacks to the
569 meteorology, thermodynamic environment and radiation budget of the Arabian Peninsula, or to the soil moisture
570 wind threshold velocities. Finally, this work also points to the need to better constrain dust concentrations in
571 numerical models, and further develop our understanding of the relationship between storm dynamics and dust
572 processes.

573 **Author contributions**

574 Jennie Bukowski (JB) and Susan C. van den Heever (SvdH) designed the experiments. JB set up and performed the
575 WRF-Chem simulations and wrote the analysis code. Both JB and SvdH contributed to the analysis of the model
576 output. JB prepared the manuscript with contributions and edits from SvdH.

577 **Competing interests**

578 The authors declare that they have no conflict of interest.

Acknowledgements

This work was funded by an Office of Naval Research – Multidisciplinary University Research Initiative (ONR-MURI) grant (# N00014-16-1-2040). Jennie Bukowski was partially supported by the Cooperative Institute for Research in the Atmosphere (CIRA) Program of Research and Scholarly Excellence (PRSE) fellowship. The simulation data are available upon request from the corresponding author, Jennie Bukowski. Initialization data for the model was provided by: National Centers for Environmental Prediction, National Weather Service, NOAA, U.S. Department of Commerce. 2000, updated daily. NCEP FNL Operational Model Global Tropospheric Analyses, continuing from July 1999. Research Data Archive at the National Center for Atmospheric Research, Computational and Informational Systems Laboratory. https://doi.org/10.5065/D6M043C6.

References

Alizadeh Choobari, O., Zawar-Reza, P., and Sturman, A.: Low level jet intensification by mineral dust aerosols, Ann. Geophys., 31, 625–632, doi:10.5194/angeo-31-625-2013, 2013.

Almazroui, M.: Calibration of TRMM rainfall climatology over Saudi Arabia during 1998–2009, Atmos. Res., 99(3–4), 400–414, doi:10.1016/J.ATMOSRES.2010.11.006, 2011.

Aoki, T., Tanaka, T. Y., Uchiyama, A., Chiba, M., Mikami, M., Yabuki, S. And Key, J. R.: Sensitivity Experiments of Direct Radiative Forcing Caused by Mineral Dust Simulated with a Chemical Transport Model, J. Meteorol. Soc. Japan. Ser. II, 83A, 315–331, doi:10.2151/jmsj.83A.315, 2005.

Arakawa, A. and Schubert, W. H.: Interaction of a Cumulus Cloud Ensemble with the Large-Scale Environment, Part I, J. Atmos. Sci., 31(3), 674–701, doi:10.1175/1520-0469(1974)031<0674:IOACCE>2.0.CO;2, 1974.

Babu, C. A., Jayakrishnan, P. R. and Varikoden, H.: Characteristics of precipitation pattern in the Arabian Peninsula and its variability associated with ENSO, Arab. J. Geosci., 9(3), 186, doi:10.1007/s12517-015-2265-x, 2016.

Baddock, M. C., Strong, C. L., Leys, J. F., Heidenreich, S. K., Tews, E. K. and McTainsh, G. H.: A visibility and total suspended dust relationship, Atmos. Environ., 89, 329–336, doi:10.1016/J.ATMOSENV.2014.02.038, 2014.

Barnard, J. C., Fast, J. D., Paredes-Miranda, G., Arnott, W. P. and Laskin, A.: Technical Note: Evaluation of the WRF-Chem "Aerosol Chemical to Aerosol Optical Properties Module" using data from the MILAGRO campaign, Atmos. Chem. Phys., 10(15), 7325–7340, doi:10.5194/acp-10-7325-2010, 2010.

Beegum, S. N., Gherboudj, I., Chaouch, N., Temimi, M. and Ghedira, H.: Simulation and analysis of synoptic scale dust storms over the Arabian Peninsula, Atmos. Res., 199, 62–81, doi:10.1016/J.ATMOSRES.2017.09.003, 2018.

Benedetti, A., Reid, J. S., Knippertz, P., Marsham, J. H., Di Giuseppe, F., Rémy, S., Basart, S., Boucher, O., Brooks, I. M., Menut, L., Mona, L., Laj, P., Pappalardo, G., Wiedensohler, A., Baklanov, A., Brooks, M., Colarco, P. R., Cuevas, E., da Silva, A., Escribano, J., Flemming, J., Huneeus, N., Jorba, O., Kazadzis, S., Kinne, S., Popp, T., Quinn, P. K., Sekiyama, T. T., Tanaka, T. and Terradellas, E.: Status and future of numerical

614   atmospheric aerosol prediction with a focus on data requirements, Atmos. Chem. Phys., 18(14), 10615–

615   10643, doi:10.5194/acp-18-10615-2018, 2018.

616 Benedetti, A., Baldasano, J. M., Basart, S., Benincasa, F., Boucher, O., Brooks, M. E., Chen, J.-P., Colarco, P. R.,

617   Gong, S., Huneeus, N., Jones, L., Lu, S., Menut, L., Morcrette, J.-J., Mulcahy, J., Nickovic, S., Pérez

618   García-Pando, C., Reid, J. S., Sekiyama, T. T., Tanaka, T. Y., Terradellas, E., Westphal, D. L., Zhang, X.-

619   Y. and Zhou, C.-H.: Operational Dust Prediction, in Mineral Dust: A Key Player in the Earth System,

620   edited by P. Knippertz and J.-B. W. Stuut, pp. 223–265, Springer Netherlands, Dordrecht., 2014.

621 Benedetti, A., Reid, J. S. and Colarco, P. R.: International Cooperative for Aerosol Prediction Workshop on Aerosol

622   Forecast Verification, Bull. Am. Meteorol. Soc., 92(11), ES48-ES53, doi:10.1175/BAMS-D-11-00105.1,

623   2011.

624 Bishop, J. K. B., Davis, R. E. and Sherman, J. T.: Robotic Observations of Dust Storm Enhancement of Carbon

625   Biomass in the North Pacific, Science (80-.)., 298(5594), 817 LP-821, doi:10.1126/science.1074961, 2002.

626 Boose, Y., Welti, A., Atkinson, J., Ramelli, F., Danielczok, A., Bingemer, H. G., Plötze, M., Sierau, B., Kanji, Z. A.

627   and Lohmann, U.: Heterogeneous ice nucleation on dust particles sourced from nine~deserts worldwide --

628   Part 1: Immersion freezing, Atmos. Chem. Phys., 16(23), 15075–15095, doi:10.5194/acp-16-15075-2016,

629   2016.

630 Bouet, C., Cautenet, G., Bergametti, G., Marticorena, B., Todd, M. C. and Washington, R.: Sensitivity of desert dust

631   emissions to model horizontal grid spacing during the Bodélé Dust Experiment 2005, Atmos. Environ., 50,

632   377–380, doi:10.1016/J.ATMOSENV.2011.12.037, 2012.

633 Bryan, G. H., and Morrison, H.: Sensitivity of a Simulated Squall Line to Horizontal Resolution and

634   Parameterization of Microphysics, MWR, 140, 202-225, doi:10.1175/MWR-D-11-00046.1, 2012.

635 Camino, C., Cuevas, E., Basart, S., Alonso-Pérez, S., Baldasano, J. M., Terradellas, E., Marticorena, B., Rodríguez,

636   S. and Berjón, A.: An empirical equation to estimate mineral dust concentrations from visibility

637   observations in Northern Africa, Aeolian Res., 16, 55–68, doi:10.1016/J.AEOLIA.2014.11.002, 2015.

638 Chou, M.-D. and Suarez, M. J.: Technical Report Series on Global Modeling and Data Assimilation A Thermal

639   Infrared Radiation Parameterization for Atmospheric Studies Revised May 2003, Nasa Tech. Memo. 15,

640   NASA, 40 pp., 1999.

641 Corr, C. A., Ziemba, L. D., Scheuer, E., Anderson, B. E., Beyersdorf, A. J., Chen, G., Crosbie, E., Moore, R. H.,

642   Shook, M., Thornhill, K. L., Winstead, E., Lawson, R. P., Barth, M. C., Schroeder, J. R., Blake, D. R. and

643   Dibb, J. E.: Observational evidence for the convective transport of dust over the Central United States, J.

644   Geophys. Res. Atmos., 121(3), 1306–1319, doi:10.1002/2015JD023789, 2016.

645 Cowie, S. M., Marsham, J. H. and Knippertz, P.: The importance of rare, high-wind events for dust uplift in northern

646   Africa, Geophys. Res. Lett., 42(19), 8208–8215, doi:10.1002/2015GL065819, 2015.

647 Dayan, U., Ziv, B., Margalit, A., Morin, E. and Sharon, D.: A severe autumn storm over the middle-east: synoptic

648   and mesoscale convection analysis, Theor. Appl. Climatol., 69(1), 103–122, doi:10.1007/s007040170038,

649   2001.

650 Dipu, S., Prabha, T. V., Pandithurai, G., Dudhia, J., Pfister, G., Rajesh, K. and Goswami, B. N.: Impact of elevated

651   aerosol layer on the cloud macrophysical properties prior to monsoon onset, Atmos. Environ., 70, 454–467,
652   doi:10.1016/J.ATMOSENV.2012.12.036, 2013.
653   Emmons, L. K., Walters, S., Hess, P. G., Lamarque, J.-F., Pfister, G. G., Fillmore, D., Granier, C., Guenther,
654   A., Kinnison, D., Laepple, T., Orlando, J., Tie, X., Tyndall, G., Wiedinmyer, C., Baughcum, S. L., and
655   Kloster, S.: Description and evaluation of the Model for Ozone and Related chemical Tracers, version 4
656   (MOZART-4), Geosci. Model Dev., 3, 43-67, doi.org/10.5194/gmd-3-43-2010, 2010. *We acknowledge use*
657   *of NCAR/ACOM CAM-chem global model output available at https://www.acom.ucar.edu/cam-chem/cam-*
658   *chem.shtml.*
659
660   Fadnavis, S., Semeniuk, K., Pozzoli, L., Schultz, M. G., Ghude, S. D., Das, S. and Kakatkar, R.: Transport of
661   aerosols into the UTLS and their impact on the Asian monsoon region as seen in a global model simulation,
662   Atmos. Chem. Phys., 13(17), 8771–8786, doi:10.5194/acp-13-8771-2013, 2013.
663   Fast, J. D., Gustafson Jr., W. I., Easter, R. C., Zaveri, R. A., Barnard, J. C., Chapman, E. G., Grell, G. A. and
664   Peckham, S. E.: Evolution of ozone, particulates, and aerosol direct radiative forcing in the vicinity of
665   Houston using a fully coupled meteorology-chemistry-aerosol model, J. Geophys. Res. Atmos., 111(D21),
666   doi:10.1029/2005JD006721, 2006.
667   Field, P. R., Möhler, O., Connolly, P., Krämer, M., Cotton, R., Heymsfield, A. J., Saathoff, H. and Schnaiter, M.:
668   Some ice nucleation characteristics of Asian and Saharan desert dust, Atmos. Chem. Phys., 6(10), 2991–
669   3006, doi:10.5194/acp-6-2991-2006, 2006.
670   Giannakopoulou, E. M. and Toumi, R.: The Persian Gulf summertime low-level jet over sloping terrain, Q. J. R.
671   Meteorol. Soc., 138(662), 145–157, doi:10.1002/qj.901, 2012.
672   Ginoux, P., Chin, M., Tegen, I., Prospero, J. M., Holben, B., Dubovik, O. and Lin, S.-J.: Sources and distributions of
673   dust aerosols simulated with the GOCART model, J. Geophys. Res. Atmos., 106(D17), 20255–20273,
674   doi:10.1029/2000JD000053, 2001.
675   Ginoux, P., Prospero, J. M., Gill, T. E., Hsu, N. C. and Zhao, M.: Global-scale attribution of anthropogenic and
676   natural dust sources and their emission rates based on MODIS Deep Blue aerosol products, Rev. Geophys.,
677   50(3), doi:10.1029/2012RG000388, 2012.
678   Grell, G. A., Peckham, S. E., Schmitz, R., McKeen, S. A., Frost, G., Skamarock, W. C. and Eder, B.: Fully coupled
679   "online" chemistry within the WRF model, Atmos. Environ., 39(37), 6957–6975,
680   doi:10.1016/J.ATMOSENV.2005.04.027, 2005.
681   Hasanean, H., Almazroui, M., Hasanean, H. and Almazroui, M.: Rainfall: Features and Variations over Saudi
682   Arabia, A Review, Climate, 3(3), 578–626, doi:10.3390/cli3030578, 2015.
683   Haywood, J. M., Allan, R. P., Culverwell, I., Slingo, T., Milton, S., Edwards, J. and Clerbaux, N.: Can desert dust
684   explain the outgoing longwave radiation anomaly over the Sahara during July 2003?, J. Geophys. Res.
685   Atmos., 110(D5), doi:10.1029/2004JD005232, 2005.
686   Heald, C. L., Ridley, D. A., Kroll, J. H., Barrett, S. R. H., Cady-Pereira, K. E., Alvarado, M. J. and Holmes, C. D.:

Contrasting the direct radiative effect and direct radiative forcing of aerosols, Atmos. Chem. Phys., 14(11), 5513–5527, doi:10.5194/acp-14-5513-2014, 2014.

Heinold, B., Knippertz, P., Marsham, J. H., Fiedler, S., Dixon, N. S., Schepanski, K., Laurent, B. and Tegen, I.: The role of deep convection and nocturnal low-level jets for dust emission in summertime West Africa: Estimates from convection-permitting simulations, J. Geophys. Res. Atmos., 118(10), 4385–4400, doi:10.1002/jgrd.50402, 2013.

Huneeus, N., Schulz, M., Balkanski, Y., Griesfeller, J., Prospero, J., Kinne, S., Bauer, S., Boucher, O., Chin, M., Dentener, F., Diehl, T., Easter, R., Fillmore, D., Ghan, S., Ginoux, P., Grini, A., Horowitz, L., Koch, D., Krol, M. C., Landing, W., Liu, X., Mahowald, N., Miller, R., Morcrette, J.-J., Myhre, G., Penner, J., Perlwitz, J., Stier, P., Takemura, T. and Zender, C. S.: Global dust model intercomparison in AeroCom phase I, Atmos. Chem. Phys., 11(15), 7781–7816, doi:10.5194/acp-11-7781-2011, 2011.

Jickells, T. and Moore, C. M.: The Importance of Atmospheric Deposition for Ocean Productivity, Annu. Rev. Ecol. Evol. Syst., 46(1), 481–501, doi:10.1146/annurev-ecolsys-112414-054118, 2015.

Jish Prakash, P., Stenchikov, G., Kalenderski, S., Osipov, S. and Bangalath, H.: The impact of dust storms on the Arabian Peninsula and the Red Sea, Atmos. Chem. Phys., 15(1), 199–222, doi:10.5194/acp-15-199-2015, 2015.

Jung, E., Shao, Y. and Sakai, T.: A study on the effects of convective transport on regional-scale Asian dust storms in 2002, J. Geophys. Res. Atmos., 110(D20), doi:10.1029/2005JD005808, 2005.

Kain, J. S.: The Kain–Fritsch Convective Parameterization: An Update, J. Appl. Meteorol., 43(1), 170–181, doi:10.1175/1520-0450(2004)043<0170:TKCPAU>2.0.CO;2, 2004.

Kalenderski, S., Stenchikov, G. and Zhao, C.: Modeling a typical winter-time dust event over the Arabian Peninsula and the Red Sea, Atmos. Chem. Phys., 13(4), 1999–2014, doi:10.5194/acp-13-1999-2013, 2013.

Kalenderski, S. and Stenchikov, G.: High-resolution regional modeling of summertime transport and impact of African dust over the Red Sea and Arabian Peninsula, J. Geophys. Res. Atmos., 121(11), 6435–6458, doi:10.1002/2015JD024480, 2016.

Karydis, V. A., Kumar, P., Barahona, D., Sokolik, I. N. and Nenes, A.: On the effect of dust particles on global cloud condensation nuclei and cloud droplet number, J. Geophys. Res. Atmos., 116(D23), doi:10.1029/2011JD016283, 2011.

Kinne, S., Lohmann, U., Feichter, J., Schulz, M., Timmreck, C., Ghan, S., Easter, R., Chin, M., Ginoux, P., Takemura, T., Tegen, I., Koch, D., Herzog, M., Penner, J., Pitari, G., Holben, B., Eck, T., Smirnov, A., Dubovik, O., Slutsker, I., Tanre, D., Torres, O., Mishchenko, M., Geogdzhayev, I., Chu, D. A. and Kaufman, Y.: Monthly averages of aerosol properties: A global comparison among models, satellite data, and AERONET ground data, J. Geophys. Res. Atmos., 108(D20), doi:10.1029/2001JD001253, 2003.

Kishcha, P., Alpert, P., Barkan, J., Kirschner, I. and Machenhauer, B.: Atmospheric response to Saharan dust deduced from ECMWF reanalysis (ERA) temperature increments, Tellus B Chem. Phys. Meteorol., 55(4), 901–913, doi:10.3402/tellusb.v55i4.16380, 2011.

Klich, C. A. and Fuelberg, H. E.: The role of horizontal model resolution in assessing the transport of CO in a

724   middle latitude cyclone using WRF-Chem, Atmos. Chem. Phys., 14(2), 609–627, doi:10.5194/acp-14-609-
725   2014, 2014.

726 Klose, M. and Shao, Y.: Stochastic parameterization of dust emission and application to convective atmospheric
727   conditions, Atmos. Chem. Phys., 12, 7309-7320, doi:10.5194/acp-12-7309-2012, 2012.

728 Knopf, D. A. and Koop, T.: Heterogeneous nucleation of ice on surrogates of mineral dust, J. Geophys. Res. Atmos.,
729   111(D12), doi:10.1029/2005JD006894, 2006.

730 Kok, J. F., Mahowald, N. M., Fratini, G., Gillies, J. A., Ishizuka, M., Leys, J. F., Mikami, M., Park, M.-S., Park, S.-
731   U., Van Pelt, R. S. and Zobeck, T. M.: An improved dust emission model – Part 1: Model description and
732   comparison against measurements, Atmos. Chem. Phys., 14(23), 13023–13041, doi:10.5194/acp-14-13023-
733   2014, 2014.

734 Kok, J. F., Ward, D. S., Mahowald, N. M. and Evan, A. T.: Global and regional importance of the direct dust-
735   climate feedback, Nat. Commun., 9(1), 241, doi:10.1038/s41467-017-02620-y, 2018.

736 Largeron, Y., Guichard, F., Bouniol, D., Couvreux, F., Kergoat, L. and Marticorena, B.: Can we use surface wind
737   fields from meteorological reanalyses for Sahelian dust emission simulations?, Geophys. Res. Lett., 42(7),
738   2490–2499, doi:10.1002/2014GL062938, 2015.

739 Lee, Y. H., Chen, K. and Adams, P. J.: Development of a global model of mineral dust aerosol microphysics,
740   Atmos. Chem. Phys., 9(7), 2441–2458, doi:10.5194/acp-9-2441-2009, 2009.

741 Liao, H. and Seinfeld, J. H.: Radiative forcing by mineral dust aerosols: Sensitivity to key variables, J. Geophys.
742   Res. Atmos., 103(D24), 31637–31645, doi:10.1029/1998JD200036, 1998.

743 Mahowald, N. M., Ballantine, J. A., Feddema, J. and Ramankutty, N.: Global trends in visibility: implications for
744   dust sources, Atmos. Chem. Phys., 7(12), 3309–3339, doi:10.5194/acp-7-3309-2007, 2007.

745 Mahowald, N. M., Baker, A. R., Bergametti, G., Brooks, N., Duce, R. A., Jickells, T. D., Kubilay, N., Prospero, J.
746   M. and Tegen, I.: Atmospheric global dust cycle and iron inputs to the ocean, Global Biogeochem. Cycles,
747   19(4), doi:10.1029/2004GB002402, 2005.

748 Manktelow, P. T., Carslaw, K. S., Mann, G. W. and Spracklen, D. V: The impact of dust on sulfate aerosol, CN and
749   CCN during an East Asian dust storm, Atmos. Chem. Phys., 10(2), 365–382, doi:10.5194/acp-10-365-
750   2010, 2010.

751 Marsham, J. H., Parker, D. J., Grams, C. M., Taylor, C. M. and Haywood, J. M.: Uplift of Saharan dust south of the
752   intertropical discontinuity, J. Geophys. Res. Atmos., 113(D21), doi:10.1029/2008JD009844, 2008.

753 Marsham, J. H., Knippertz, P., Dixon, N. S., Parker, D. J. and Lister, G. M. S.: The importance of the representation
754   of deep convection for modeled dust-generating winds over West Africa during summer, Geophys. Res.
755   Lett., 38(16), doi:10.1029/2011GL048368, 2011.

756 Marticorena, B. and Bergametti, G.: Modeling the atmospheric dust cycle: 1. Design of a soil-derived dust emission
757   scheme, J. Geophys. Res. Atmos., 100(D8), 16415–16430, doi:10.1029/95JD00690, 1995.

758 Martin, J. H.: Iron still comes from above, Nature, 353(6340), 123, doi:10.1038/353123b0, 1991.

759 Menut, L.: Sensitivity of hourly Saharan dust emissions to NCEP and ECMWF modeled wind speed, J. Geophys.
760   Res. Atmos., 113(D16), doi:10.1029/2007JD009522, 2008.

761   Miller, S. D., Grasso, L., Bian, Q., Kreidenweis, S., Dostalek, J., Solbrig, J., Bukowski, J., van den Heever, S. C.,

762   Wang, Y., Xu, X., Wang, J., Walker, A., Wu, T.-C., Zupanski, M., Chiu, C., and Reid, J.: *A Tale of Two*

763   *Dust Storms*: Analysis of a Complex Dust Event in the Middle East, Atmos. Meas. Tech. Discuss.,

764   doi:10.5194/amt-2019-82, 2019.

765   Miller, S. D., Kuciauskas, A. P., Liu, M., Ji, Q., Reid, J. S., Breed, D. W., Walker, A. L. and Mandoos, A. Al:

766   Haboob dust storms of the southern Arabian Peninsula, J. Geophys. Res. Atmos., 113(D1),

767   doi:10.1029/2007JD008550, 2008.

768   Morrison, H., Curry, J. A. and Khvorostyanov, V. I.: A New Double-Moment Microphysics Parameterization for

769   Application in Cloud and Climate Models. Part I: Description, J. Atmos. Sci., 62(6), 1665–1677,

770   doi:10.1175/JAS3446.1, 2005.

771   Morrison, H., Thompson, G. and Tatarskii, V.: Impact of Cloud Microphysics on the Development of Trailing

772   Stratiform Precipitation in a Simulated Squall Line: Comparison of One- and Two-Moment Schemes, Mon.

773   Weather Rev., 137(3), 991–1007, doi:10.1175/2008MWR2556.1, 2009.

774   Nakanishi, M. and Niino, H.: An Improved Mellor--Yamada Level-3 Model: Its Numerical Stability and Application

775   to a Regional Prediction of Advection Fog, Boundary-Layer Meteorol., 119(2), 397–407,

776   doi:10.1007/s10546-005-9030-8, 2006.

777   Nakanishi, M. and NIINO, H.: Development of an Improved Turbulence Closure Model for the Atmospheric

778   Boundary Layer, J. Meteorol. Soc. Japan. Ser. II, 87(5), 895–912, doi:10.2151/jmsj.87.895, 2009.

779   National Centers for Environmental Prediction/National Weather Service/NOAA/U.S. Department of Commerce:

780   NCEP GDAS/FNL 0.25 Degree Global Tropospheric Analyses and Forecast Grids, Research Data Archive

781   at the National Center for Atmospheric Research, Computational and Information Systems Laboratory,

782   Boulder, CO, https://doi.org/10.5065/D65Q4T4Z, 2015.

783   Niu, G.-Y., Yang, Z.-L., Mitchell, K. E., Chen, F., Ek, M. B., Barlage, M., Kumar, A., Manning, K., Niyogi, D.,

784   Rosero, E., Tewari, M. and Xia, Y.: The community Noah land surface model with multiparameterization

785   options (Noah-MP): 1. Model description and evaluation with local-scale measurements, J. Geophys. Res.

786   Atmos., 116(D12), doi:10.1029/2010JD015139, 2011.

787   Pantillon, F., Knippertz, P., Marsham, J. H. and Birch, C. E.: A Parameterization of Convective Dust Storms for

788   Models with Mass-Flux Convection Schemes, J. Atmos. Sci., 72(6), 2545–2561, doi:10.1175/JAS-D-14-

789   0341.1, 2015.

790   Pantillon, F., Knippertz, P., Marsham, J. H., Panitz, H.-J. and Bischoff-Gauss, I.: Modeling haboob dust storms in

791   large-scale weather and climate models, J. Geophys. Res. Atmos., 121(5), 2090–2109,

792   doi:10.1002/2015JD024349, 2016.

793   Pérez, C., Nickovic, S., Pejanovic, G., Baldasano, J. M. and Özsoy, E.: Interactive dust-radiation modeling: A step

794   to improve weather forecasts, J. Geophys. Res. Atmos., 111(D16), doi:10.1029/2005JD006717, 2006.

795   Pope, R. J., Marsham, J. H., Knippertz, P., Brooks, M. E. and Roberts, A. J.: Identifying errors in dust models from

796   data assimilation, Geophys. Res. Lett., 43(17), 9270–9279, doi:10.1002/2016GL070621, 2016.

797   Prospero, J. M.: Long-term measurements of the transport of African mineral dust to the southeastern United States:

798   Implications for regional air quality, J. Geophys. Res. Atmos., 104(D13), 15917–15927,

799   doi:10.1029/1999JD900072, 1999.

800 Reid, J. S., Benedetti, A., Colarco, P. R. and Hansen, J. A.: International Operational Aerosol Observability

801   Workshop, Bull. Am. Meteorol. Soc., 92(6), ES21-ES24, doi:10.1175/2010BAMS3183.1, 2010.

802 Reinfried, F., Tegen, I., Heinold, B., Hellmuth, O., Schepanski, K., Cubasch, U., Huebener, H. and Knippertz, P.:

803   Simulations of convectively-driven density currents in the Atlas region using a regional model: Impacts on

804   dust emission and sensitivity to horizontal resolution and convection schemes, J. Geophys. Res. Atmos.,

805   114(D8), doi:10.1029/2008JD010844, 2009.

806 Ridley, D. A., Heald, C. L., Pierce, J. R. and Evans, M. J.: Toward resolution-independent dust emissions in global

807   models: Impacts on the seasonal and spatial distribution of dust, Geophys. Res. Lett., 40(11), 2873–2877,

808   doi:10.1002/grl.50409, 2013.

809 Roberts, A. J., Woodage, M. J., Marsham, J. H., Highwood, E. J., Ryder, C. L., McGinty, W., Wilson, S., and

810   Crook, J.: Can explicit convection improve modelled dust in summertime West Africa?, Atmos. Chem.

811   Phys., 18, 9025-9048, https://doi.org/10.5194/acp-18-9025-2018, 2018.

812 Saleeby, S. M., van den Heever, S. C., Bukowski, J., Walker, A. L., Solbrig, J. E., Atwood, S. A., Bian, Q.,

813   Kreidenweis, S. M., Wang, Y., Wang, J. and Miller, S. D.: The Influence of Simulated Surface Dust

814   Lofting Erodible Fraction on Radiative Forcing, Atmos. Chem. Phys. Discuss., 2019, 1–35,

815   doi:10.5194/acp-2018-1302, 2019.

816 Schepanski, K., Knippertz, P., Fiedler, S., Timouk, F. and Demarty, J.: The sensitivity of nocturnal low-level jets

817   and near-surface winds over the Sahel to model resolution, initial conditions and boundary-layer set-up.

818   Q.J.R. Meteorol. Soc., 141, 1442-1456. doi:10.1002/qj.2453, 2015.

819 Seigel, R. B. and van den Heever, S. C.: Dust Lofting and Ingestion by Supercell Storms, J. Atmos. Sci., 69(5),

820   1453–1473, doi:10.1175/JAS-D-11-0222.1, 2012.

821 Sessions, W. R., Reid, J. S., Benedetti, A., Colarco, P. R., da Silva, A., Lu, S., Sekiyama, T., Tanaka, T. Y.,

822   Baldasano, J. M., Basart, S., Brooks, M. E., Eck, T. F., Iredell, M., Hansen, J. A., Jorba, O. C., Juang, H.-

823   M. H., Lynch, P., Morcrette, J.-J., Moorthi, S., Mulcahy, J., Pradhan, Y., Razinger, M., Sampson, C. B.,

824   Wang, J. and Westphal, D. L.: Development towards a global operational aerosol consensus: basic

825   climatological characteristics of the International Cooperative for Aerosol Prediction Multi-Model

826   Ensemble (ICAP-MME), Atmos. Chem. Phys., 15(1), 335–362, doi:10.5194/acp-15-335-2015, 2015.

827 Shwehdi, M. H.: Thunderstorm distribution and frequency in Saudi Arabia, J. Geophys. Eng., 2(3), 252–267,

828   doi:10.1088/1742-2132/2/3/009, 2005.

829 Skamarock, W. C., Klemp, J. B., Dudhia, J. O. G. D., and Barker, D. M.: A description of the Advanced Research

830   WRF version 3, NCAR Tech. Note NCAR/TN-4751STR, NCAR, http://dx.doi.org/10.5065/D68S4MVH,

831   Boulder, CO, 2008.

832 Slingo, A., Ackerman, T. P., Allan, R. P., Kassianov, E. I., McFarlane, S. A., Robinson, G. J., Barnard, J. C., Miller,

833   M. A., Harries, J. E., Russell, J. E. and Dewitte, S.: Observations of the impact of a major Saharan dust

834   storm on the atmospheric radiation balance, Geophys. Res. Lett., 33(24), doi:10.1029/2006GL027869,

835   2006.

836 Sokolik, I. N. and Toon, O. B.: Direct radiative forcing by anthropogenic airborne mineral aerosols, Nature,

837   381(6584), 681–683, doi:10.1038/381681a0, 1996.

838 Stafoggia, M., Zauli-Sajani, S., Pey, J., Samoli, E., Alessandrini, E., Basagaña, X., Cernigliaro, A., Chiusolo, M.,

839   Demaria, M., Díaz, J., Faustini, A., Katsouyanni, K., Kelessis, A. G., Linares, C., Marchesi, S., Medina, S.,

840   Pandolfi, P., Pérez, N., Querol, X., Randi, G., Ranzi, A., Tobias, A., Forastiere, F. and null null: Desert

841   Dust Outbreaks in Southern Europe: Contribution to Daily PM_{10} Concentrations and Short-Term

842   Associations with Mortality and Hospital Admissions, Environ. Health Perspect., 124(4), 413–419,

843   doi:10.1289/ehp.1409164, 2016.

844 Stephens, G. L., L'Ecuyer, T., Forbes, R., Gettelmen, A., Golaz, J.-C., Bodas-Salcedo, A., Suzuki, K., Gabriel, P.,

845   and Haynes, J.: Dreary state of precipitation in global models, J. Geophys. Res., 115, D24211,

846   doi:10.1029/2010JD014532, 2010.

847 Sun, Y., Solomon, S., Dai, A., and Portmann, R. W.: How often does it rain? J. Clim., 19, 916–934,

848   doi:10.1175/JCLI3672.1, 2006.

849 Takemi, T.: Importance of the Numerical Representation of Shallow and Deep Convection for Simulations of

850   Dust Transport over a Desert Region, Adv. Meteorol., vol. 2012, 1-13, doi: 10.1155/2012/413584, 2012.

851 Tanaka, T. Y. and Chiba, M.: A numerical study of the contributions of dust source regions to the global dust

852   budget, Glob. Planet. Change, 52(1–4), 88–104, doi:10.1016/J.GLOPLACHA.2006.02.002, 2006.

853 Tegen, I. and Lacis, A. A.: Modeling of particle size distribution and its influence on the radiative properties of

854   mineral dust aerosol, J. Geophys. Res. Atmos., 101(D14), 19237–19244, doi:10.1029/95JD03610, 1996.

855 Teixeira, J. C., Carvalho, A. C., Tuccella, P., Curci, G. and Rocha, A.: WRF-chem sensitivity to vertical resolution

856   during a saharan dust event, Phys. Chem. Earth, Parts A/B/C, 94, 188–195,

857   doi:10.1016/J.PCE.2015.04.002, 2016.

858 Todd, M. C., Bou Karam, D., Cavazos, C., Bouet, C., Heinold, B., Baldasano, J. M., Cautenet, G., Koren, I., Perez,

859   C., Solmon, F., Tegen, I., Tulet, P., Washington, R. and Zakey, A.: Quantifying uncertainty in estimates of

860   mineral dust flux: An intercomparison of model performance over the Bodélé Depression, northern Chad, J.

861   Geophys. Res. Atmos., 113(D24), doi:10.1029/2008JD010476, 2008.

862 Tulet, P., Crahan-Kaku, K., Leriche, M., Aouizerats, B. and Crumeyrolle, S.: Mixing of dust aerosols into a

863   mesoscale convective system: Generation, filtering and possible feedbacks on ice anvils, Atmos. Res.,

864   96(2–3), 302–314, doi:10.1016/J.ATMOSRES.2009.09.011, 2010.

865 Twohy, C. H., Kreidenweis, S. M., Eidhammer, T., Browell, E. V, Heymsfield, A. J., Bansemer, A. R., Anderson, B.

866   E., Chen, G., Ismail, S., DeMott, P. J. and Van Den Heever, S. C.: Saharan dust particles nucleate droplets

867   in eastern Atlantic clouds, Geophys. Res. Lett., 36(1), doi:10.1029/2008GL035846, 2009.

868 Uno, I., Wang, Z., Chiba, M., Chun, Y. S., Gong, S. L., Hara, Y., Jung, E., Lee, S.-S., Liu, M., Mikami, M., Music,

869   S., Nickovic, S., Satake, S., Shao, Y., Song, Z., Sugimoto, N., Tanaka, T. and Westphal, D. L.: Dust model

870   intercomparison (DMIP) study over Asia: Overview, J. Geophys. Res. Atmos., 111(D12),

871   doi:10.1029/2005JD006575, 2006.

872   van Donkelaar, A., Martin, R. V, Brauer, M., Kahn, R., Levy, R., Verduzco, C. and Villeneuve, P. J.: Global

873   estimates of ambient fine particulate matter concentrations from satellite-based aerosol optical depth:

874   development and application, Environ. Health Perspect., 118(6), 847–855, doi:10.1289/ehp.0901623, 2010.

875   Woodage, M. J. and Woodward, S.: U.K. HiGEM: Impacts of Desert Dust Radiative Forcing in a High-Resolution

876   Atmospheric GCM, J. Clim., 27(15), 5907–5928, doi:10.1175/JCLI-D-13-00556.1, 2014.

877   Yang, Q., Easter, R. C., Campuzano-Jost, P., Jimenez, J. L., Fast, J. D., Ghan, S. J., Wang, H., Berg, L. K., Barth,

878   M. C., Liu, Y., Shrivastava, M. B., Singh, B., Morrison, H., Fan, J., Ziegler, C. L., Bela, M., Apel, E.,

879   Diskin, G. S., Mikoviny, T. and Wisthaler, A.: Aerosol transport and wet scavenging in deep convective

880   clouds: A case study and model evaluation using a multiple passive tracer analysis approach, J. Geophys.

881   Res. Atmos., 120(16), 8448–8468, doi:10.1002/2015JD023647, 2015.

882   Yang, Z.-L., Niu, G.-Y., Mitchell, K. E., Chen, F., Ek, M. B., Barlage, M., Longuevergne, L., Manning, K., Niyogi,

883   D., Tewari, M. and Xia, Y.: The community Noah land surface model with multiparameterization options

884   (Noah-MP): 2. Evaluation over global river basins, J. Geophys. Res. Atmos., 116(D12),

885   doi:10.1029/2010JD015140, 2011.

886   Yin, Y., Chen, Q., Jin, L., Chen, B., Zhu, S. and Zhang, X.: The effects of deep convection on the concentration and

887   size distribution of aerosol particles within the upper troposphere: A case study, J. Geophys. Res. Atmos.,

888   117(D22), doi:10.1029/2012JD017827, 2012.

889   Yu, Y., Notaro, M., Kalashnikova, O. V and Garay, M. J.: Climatology of summer Shamal wind in the Middle East,

890   J. Geophys. Res. Atmos., 121(1), 289–305, doi:10.1002/2015JD024063, 2016.

891   Yuter, S. E. and Houze, R. A.: Three-Dimensional Kinematic and Microphysical Evolution of Florida

892   Cumulonimbus. Part II: Frequency Distributions of Vertical Velocity, Reflectivity, and Differential

893   Reflectivity, Mon. Weather Rev., 123(7), 1941–1963, doi:10.1175/1520-

894   0493(1995)123<1941:TDKAME>2.0.CO;2, 1995.

895   Zender, C. S., Miller, R. L. R. L. and Tegen, I.: Quantifying mineral dust mass budgets:Terminology, constraints,

896   and current estimates, Eos, Trans. Am. Geophys. Union, 85(48), 509–512, doi:10.1029/2004EO480002,

897   2004.

898   Zhao, C., Liu, X., Leung, L. R., Johnson, B., McFarlane, S. A., Gustafson Jr., W. I., Fast, J. D. and Easter, R.: The

899   spatial distribution of mineral dust and its shortwave radiative forcing over North Africa: modeling

900   sensitivities to dust emissions and aerosol size treatments, Atmos. Chem. Phys., 10(18), 8821–8838,

901   doi:10.5194/acp-10-8821-2010, 2010.

902

WRF-Chem Version 3.9.1.1	Parameterization / Model Option
Simulation Start	02-Aug-2016-00:00:00 UTC
Simulation End	05-Aug-2016-00:00:00 UTC
Domains	dx = dy = 45km / 15km / 3km
Nesting	One-way
Vertical Levels	50 stretched
Initialization	GDAS-FNL Reanalysis
Aerosol Module / Erodible Grid Map	GOCART / Ginoux et al. (2004)
Microphysics	Morrison 2-Moment
Radiation	RRTMG Longwave & Goddard Shortwave
Land Surface	Noah-MP Land Surface Model
Cumulus Schemes **(45 km and 15 km grids only)**	Betts–Miller–Janjic (BMJ) Kain–Fritsch (KF) Grell 3D Ensemble (GD) Tiedtke Scheme (TD) Simplified Arakawa–Schubert (AS)
Boundary Layer / Surface Layer	MYNN Level 3

903   **Table 1: Summary of WRF-Chem model options utilized and the simulation setup.**
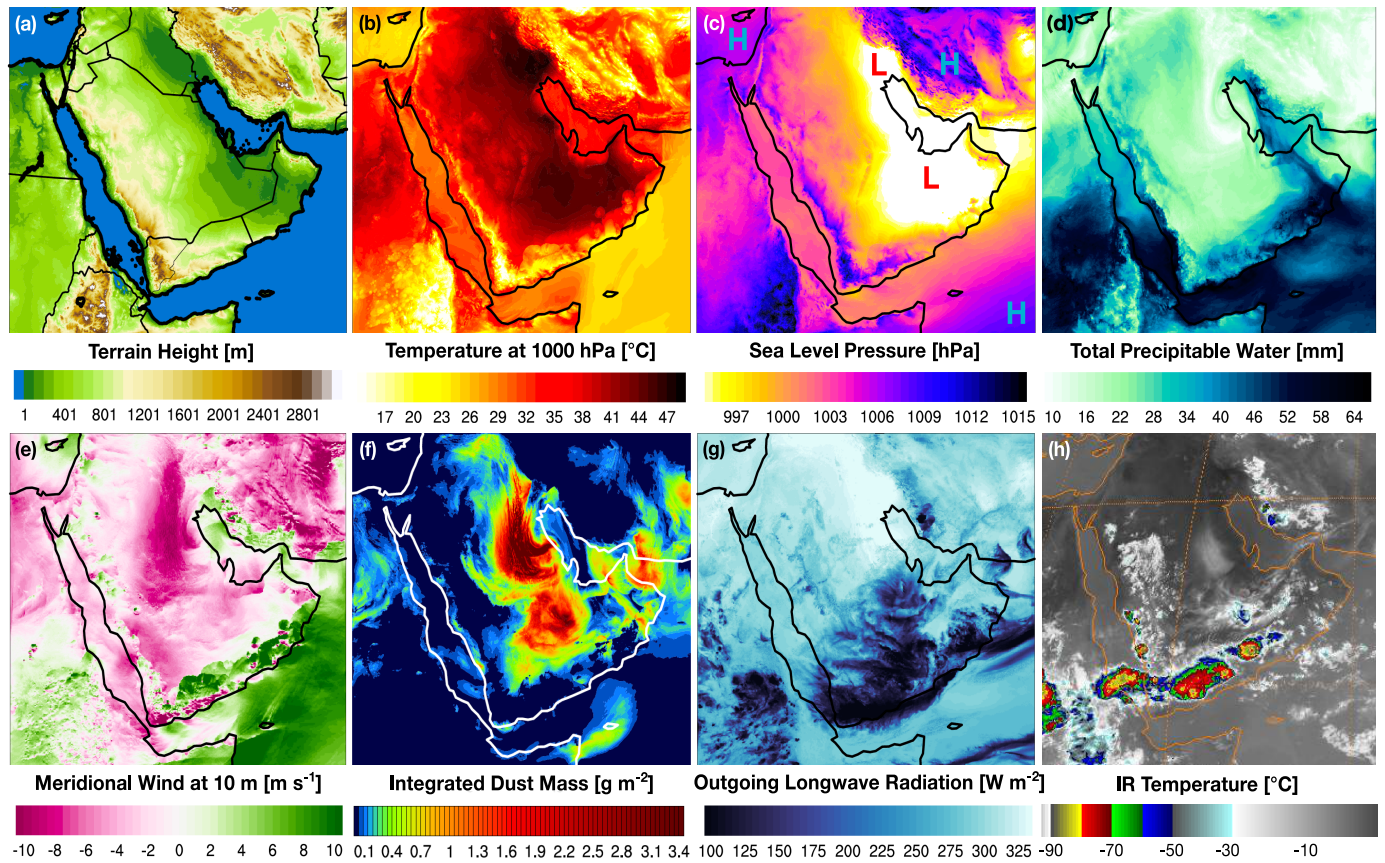
Figure 1: Case study topography and meteorology for August 3, 2016 at 15:00 UTC: (a) terrain height and national boundaries, (b) 1000 hPa Temperature, (c) sea level pressure, (d) total precipitable water, (e) meridional winds at 10 m AGL, (f) vertically integrated dust mass, (g) outgoing longwave radiation, and (h) IR temperature. Panel (h) is observed from Meteosat-7 while panels (a-g) are snapshots from the 3 km WRF-Chem simulation

909
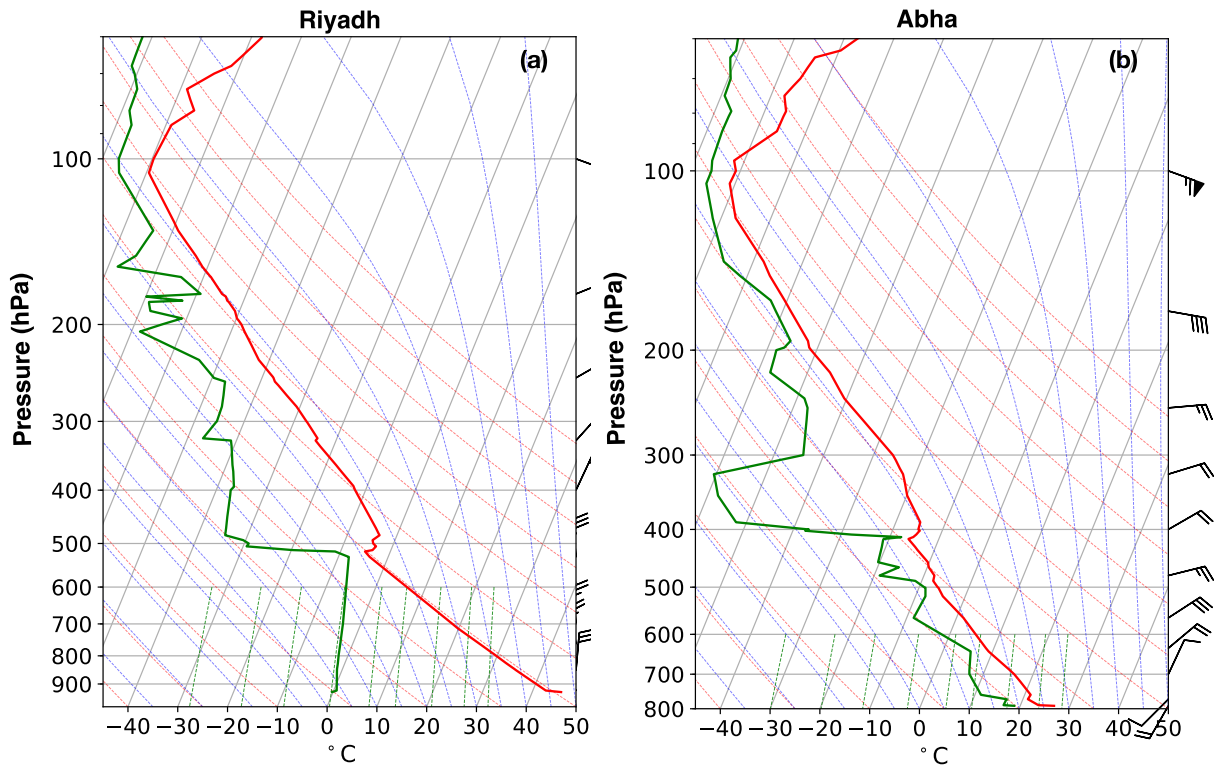
910 **Figure 2. Skew-T diagrams for two radiosonde release sites in Saudi Arabia on August 3, 2016 at 12:00 UTC for an inland**

911 **location (a) and a location nearer to the coast (b).**

912

913
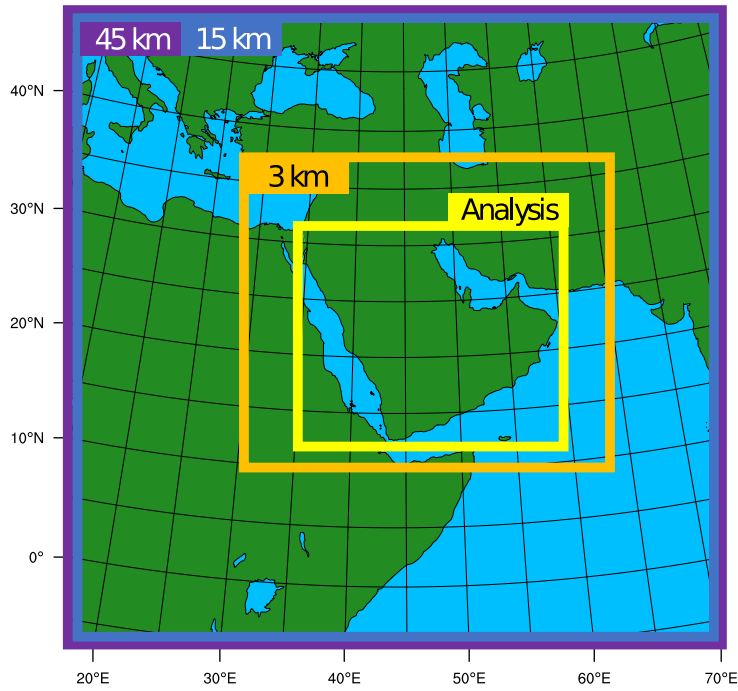
Figure 3: Model domain setup and analysis region for the 45 km (purple) and 15 km (blue) independent simulations with cumulus parameterizations, and the 3 km nested convection permitting simulation (orange). The averaging region for the analysis is denoted in yellow.

917
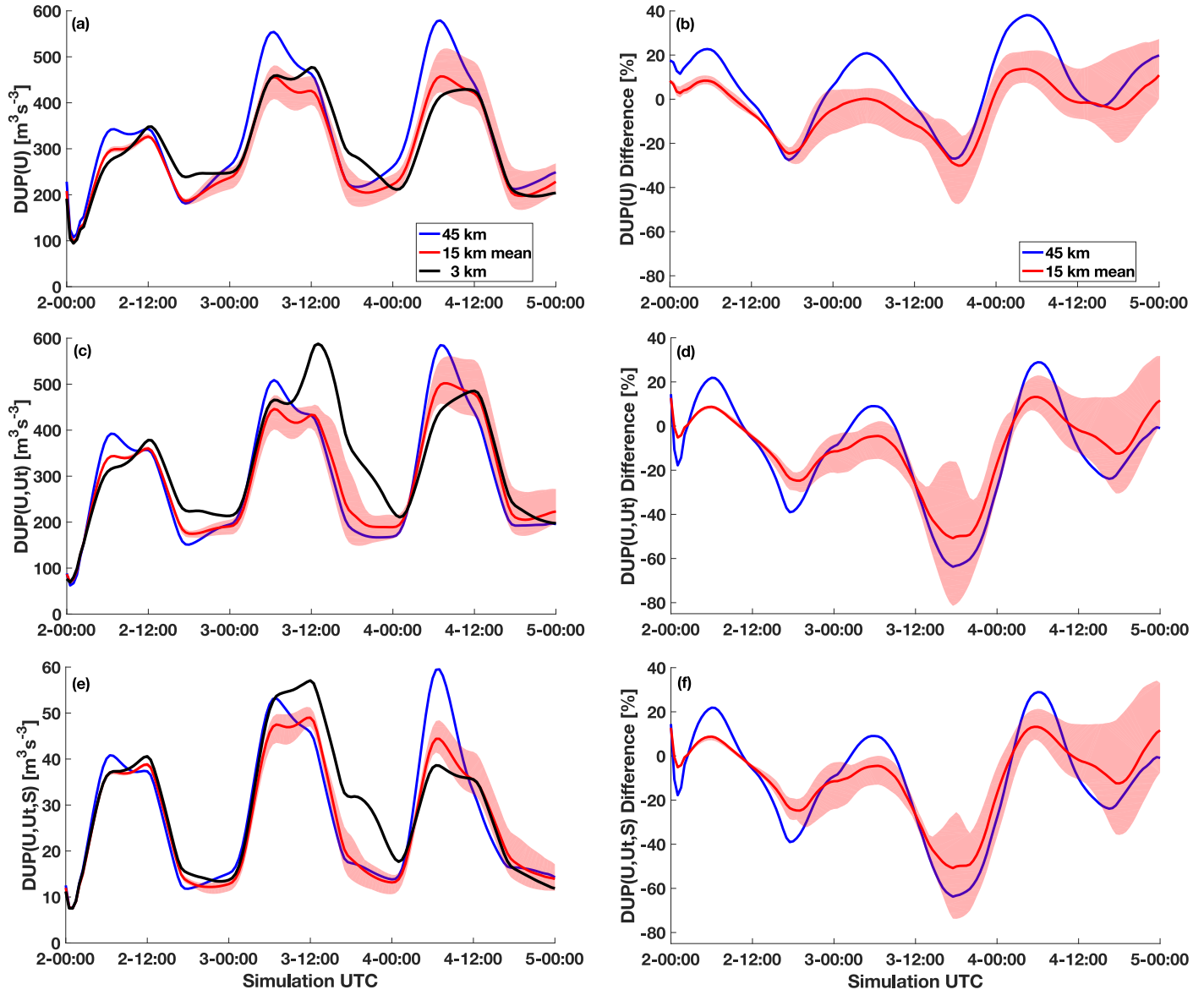
918 **Figure 4: Left column: spatially averaged dust uplift potential for (a) DUP(U), (c) DUP(U,U$_t$), and (e) DUP(U,U$_t$,S) for the**

919 **45 km (blue), 15 km mean (red), and 3 km (black) simulations with the maximum and minimum spread across the 15 km**

920 **simulations indicated in light red shading. Note that in panel (e) there is a change in scale in the ordinate. Right column:**

921 **percent difference between the 3 km convection-permitting simulation and the simulations employing cumulus**

922 **parameterizations for the different DUP parameters.**

923
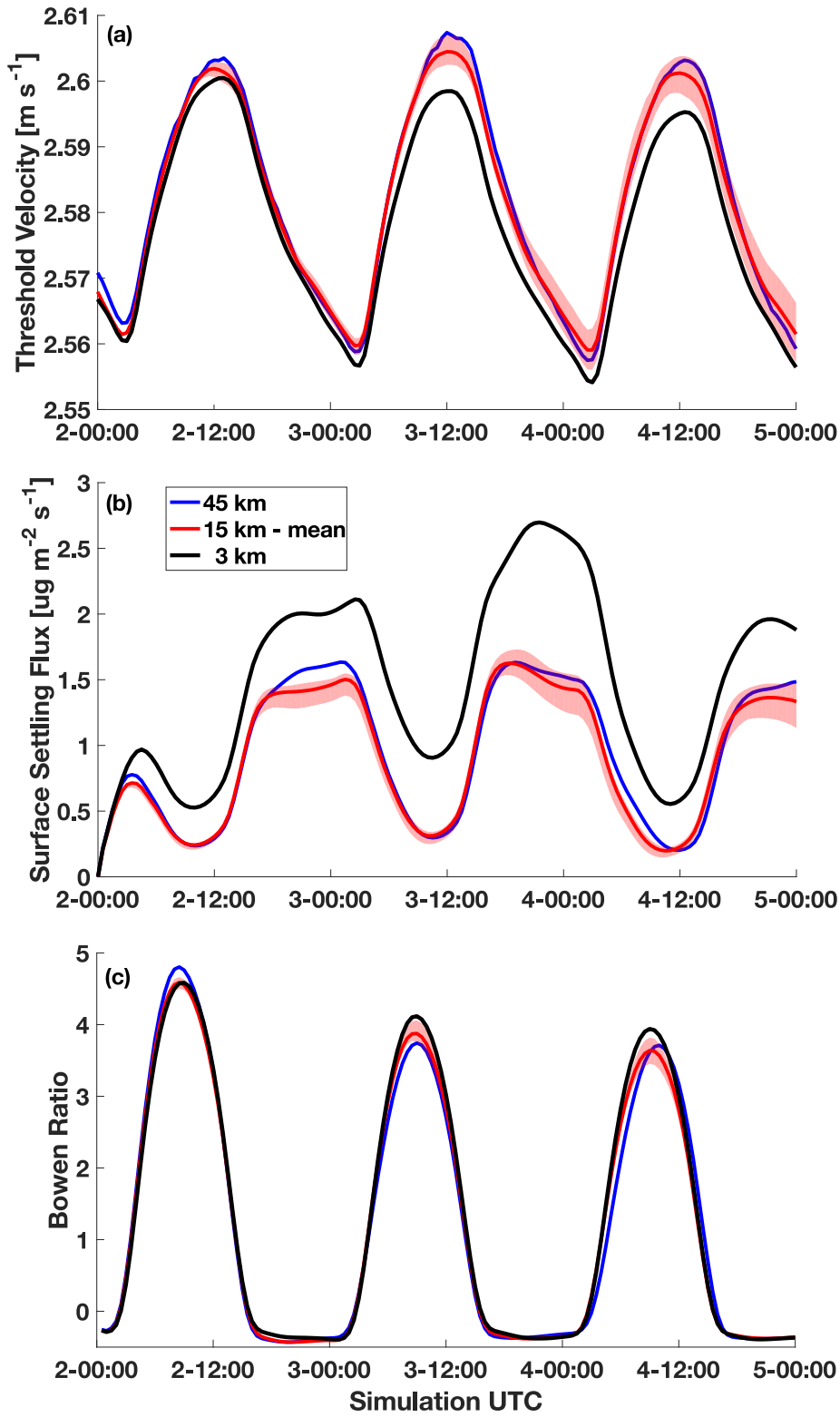
924 **Figure 5: Spatially averaged (a) dust uplift threshold velocity, (b) dust surface settling flux, and (c) Bowen ratio of**
925 **sensible to latent heat flux. Colors and shading are the same as in Fig. 4.**

926
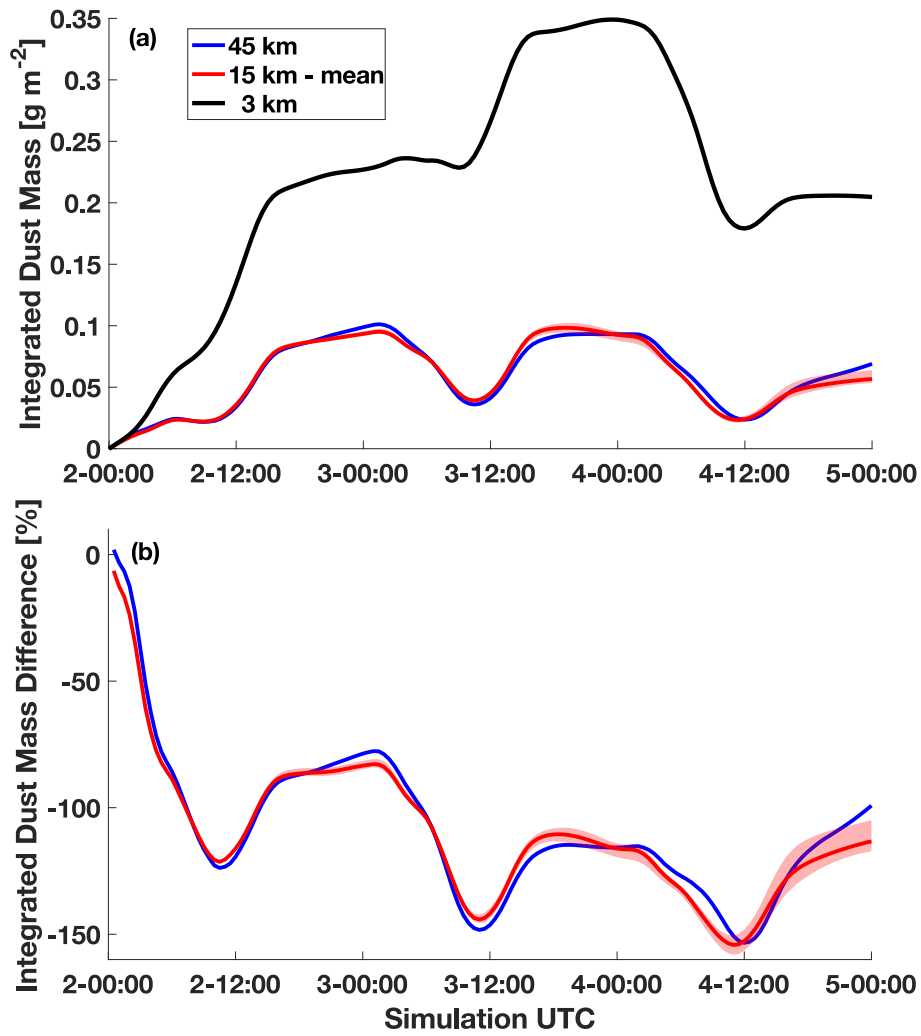
927   **Figure 6: Spatially averaged, vertically integrated dust mass. Colors and shading are identical to that in previous figures.**

928
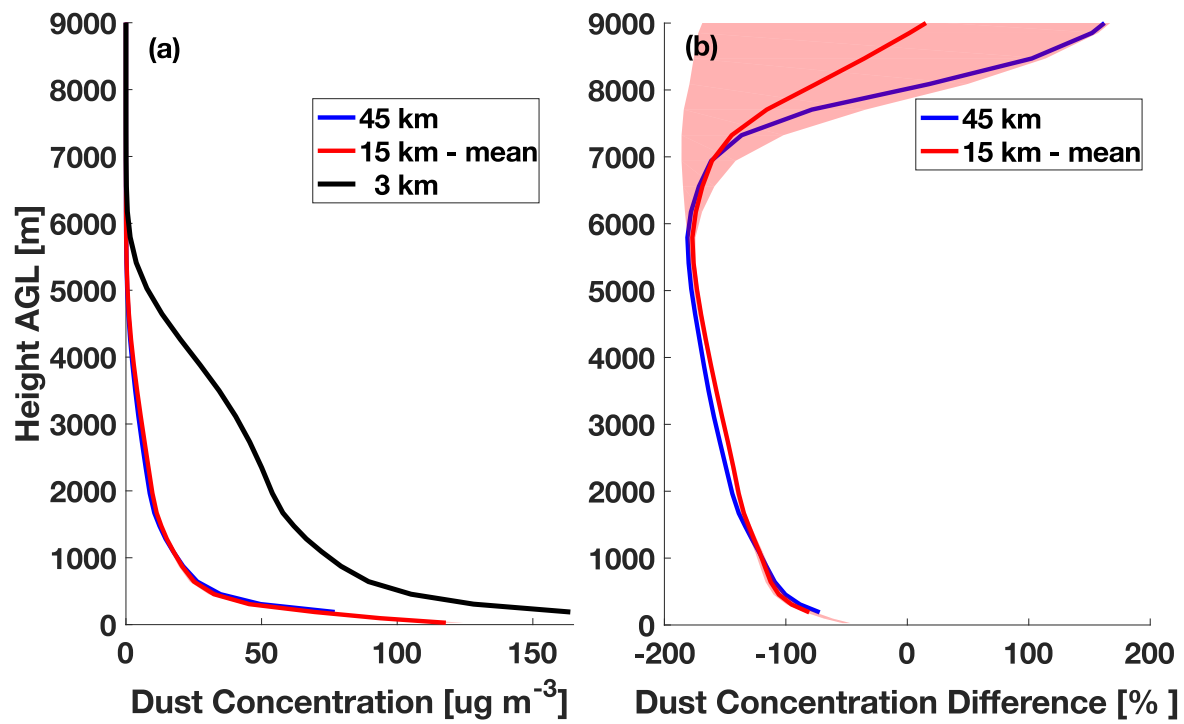
929 **Figure 7: Spatially and time averaged vertical dust concentrations (a), with the (b) percent difference between the 3 km**
930 **convection-permitting simulation and the simulations employing cumulus parameterizations. Plots are truncated at 9 km**
931 **since the values above this height do not significantly vary from what is shown here. Colors and shading are identical to**
932 **that in previous figures.**

933
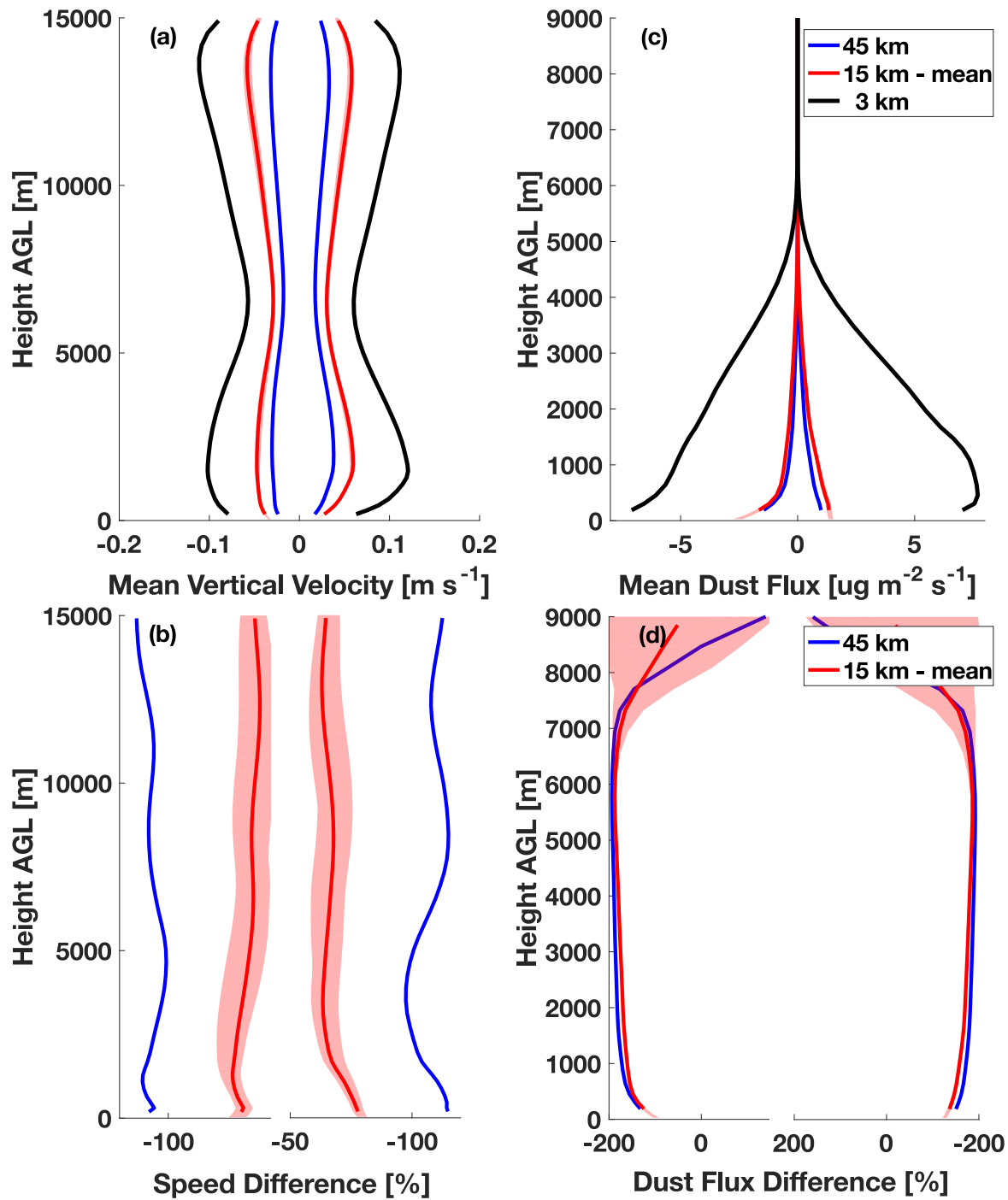
Figure 8. Left column: spatially and time averaged vertical velocities (a), with the (b) percent difference between the 3 km convection-permitting simulation and the simulations employing cumulus parameterizations. All velocities above or below zero were considered. Colors and shading are identical to that in previous figures. Right column: same but for vertical dust mass flux. Note that in panels (c) and (d) the vertical axes are truncated at 9 km since the values above this height do not significantly vary from what is shown here.

940
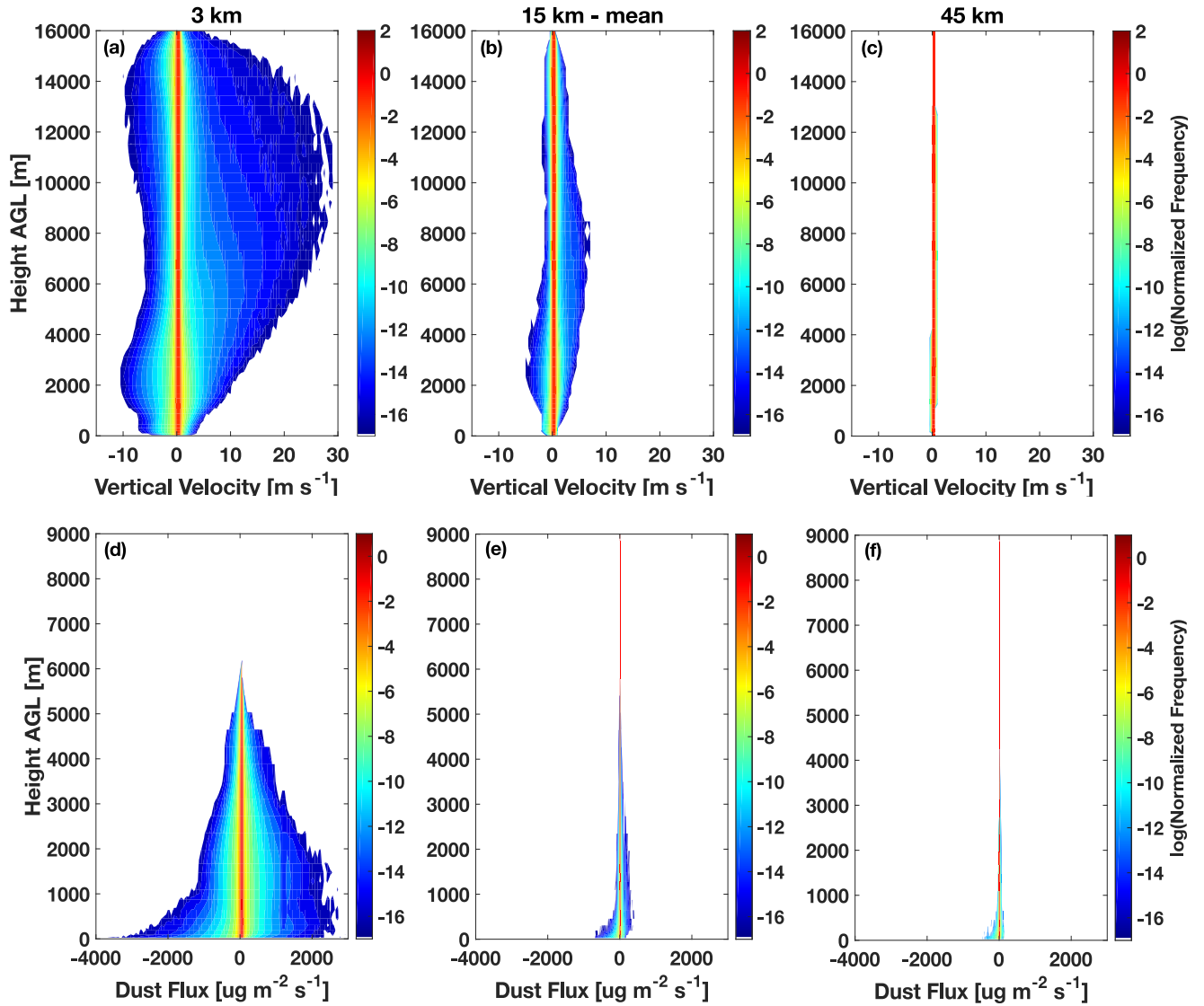
Figure 9: Top row: Contoured Frequency by Altitude Diagrams (CFADs) for vertical velocity, normalized by the number of grid points in each respective simulation. The contours are computed on a log scale to highlight the variances away from zero. Bottom row: same but for vertical dust mass flux. Note that the panels in the bottom row are truncated at 9 km since the values above this height do not significantly vary from what is shown here.

945
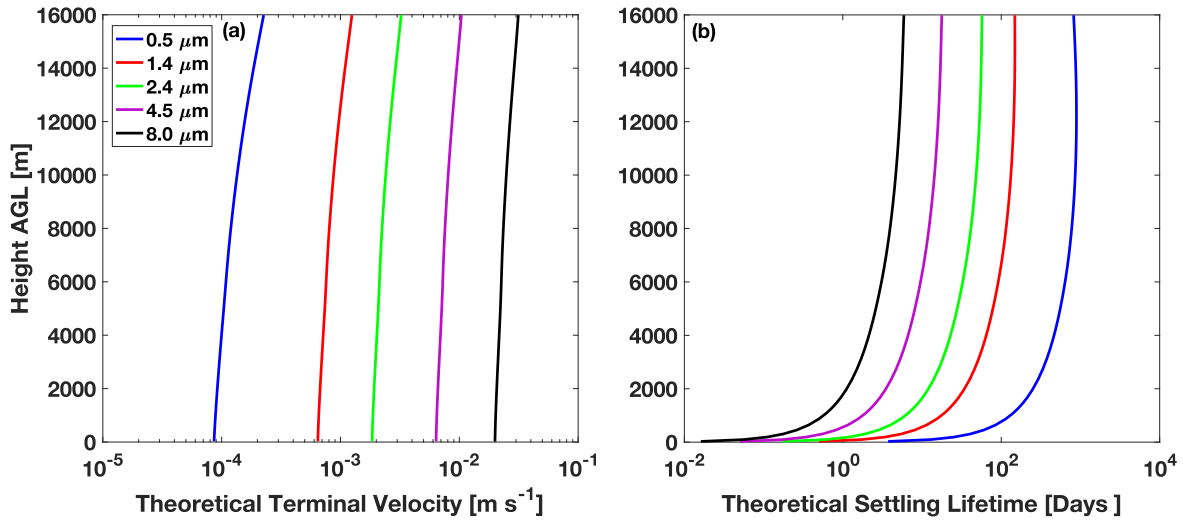
946 Figure 10: Theoretical terminal velocity of dust particles (a) based on Stokes settling velocity with slip correction for
947 pressure dependence for the 5 effective radii of dust particles in WRF-Chem. The calculations assume no vertical
948 motions, advection, deposition, coagulation, or condensation. (b) The lifetime of these theoretical dust particles based on
949 their height in the atmosphere.

950

951
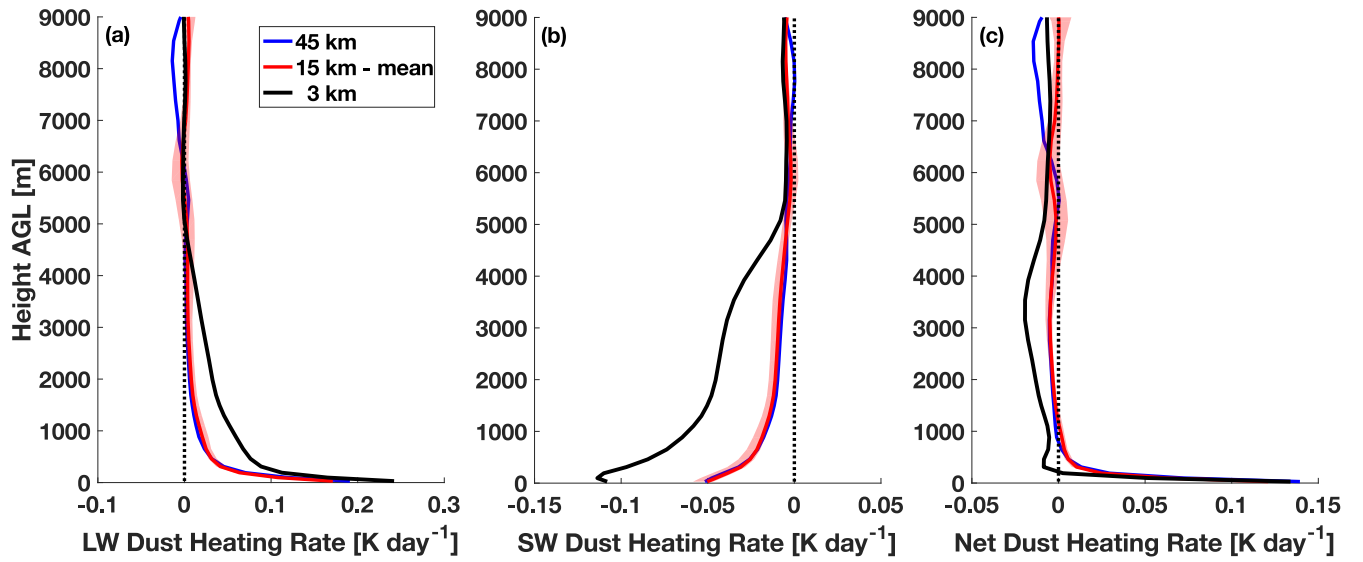
Figure 11: Spatially and time averaged longwave (a), shortwave (b), and net (c) dust heating rate profile for the 45 km

(blue), 15 km mean (red), and 3 km (black) simulations with the maximum and minimum spread across the 15 km

simulations indicated in light red shading. Plots are truncated at 9 km since the values above this height do not

significantly vary from what is shown here.